nagra.

Technical Report 09-04

A Review of the Possible Effects of Hydrogen on Lifetime of Carbon Steel Nuclear Waste Canisters

July 2009

Alan Turnbull

National Physical Laboratory, UK

National Cooperative
for the Disposal of
Radioactive Waste

Hardstrasse 73
CH-5430 Wettingen
Switzerland
Tel. +41 56 437 11 11

www.nagra.ch

nagra.

Technical Report 09-04

A Review of the Possible Effects of Hydrogen on Lifetime of Carbon Steel Nuclear Waste Canisters

July 2009

Alan Turnbull

National Physical Laboratory, UK

National Physical Laboratory
Hampton Road, Teddington, Middlesex, TW11 0LW

National Cooperative
for the Disposal of
Radioactive Waste

Hardstrasse 73
CH-5430 Wettingen
Switzerland
Tel. +41 56 437 11 11

www.nagra.ch

This report was prepared on behalf of Nagra. The viewpoints presented and conclusions reached are those of the author(s) and do not necessarily represent those of Nagra.

ISSN 1015-2636

Abstract

In Switzerland, the National Cooperative for the Disposal of Radioactive Waste (Nagra) is responsible for developing an effective method for the safe disposal of vitrified high level waste (HLW) and spent fuel. One of the options for disposal canisters is thick-walled carbon steel. The canisters, which would have a diameter of about 1 m and a length of about 3 m (HLW) or about 5 m (spent fuel), will be embedded in horizontal tunnels and surrounded with bentonite clay. The regulatory requirement for the minimum canister lifetime is 1'000 years but demonstration of a minimum lifetime of 10'000 years would be desirable. The pore-water to which the canister will be exposed is of marine origin with about 0.1-0.3 M Cl^-. Since hydrogen is generated during the corrosion process, it is necessary to assess the probability of hydrogen assisted cracking modes and to make recommendations to eliminate that probability.

To that aim, key reports detailing projections for the local environment and associated corrosion rate of the waste canister have been evaluated with the focus on the implication for the absorbed hydrogen concentration in the steel. Simple calculations of hydrogen diffusion and accumulation in the inner compartment of the sealed canister indicate that a pressure equivalent to that for gas pockets external to the canister (envisaged to be about 10 MPa) may be attained in the proposed exposure time, an important consideration since it is not possible to modify the internal surface of the closure weld. Current ideas on mechanisms of hydrogen assisted cracking are assessed from which it is concluded that the mechanistic understanding and associated models of hydrogen assisted cracking are insufficient to provide a framework for quantitative prediction for this application. The emphasis then was to identify threshold conditions for cracking and to evaluate the likelihood that these may be exceeded over the lifetime of the containment. Based on an analysis of data in the context of the waste canisters it is concluded that the likelihood of cracking due to absorbed hydrogen is remote. Recommendations are given for selection of steel composition, processing and welding procedures to eliminate effectively the probability of cracking for the assumed operational conditions for the disposal canister.

Zusammenfassung

In der Schweiz ist die Nationale Genossenschaft für die Lagerung radioaktiver Abfälle (Nagra) zuständig für die Erarbeitung einer geeigneten Lösung zur sicheren Entsorgung der verglasten hochaktiven Abfälle (HAA) und abgebrannten Brennelemente (BE). Eine mögliche Option für die Lagerbehälter ist dickwandiger Kohlenstoffstahl. Die Lagerbehälter weisen einen Durchmesser von etwa 1 m und eine Länge von etwa 3 m (HAA) bzw. 5 m (BE) auf und werden in horizontale Stollen eingelagert, welche mit Bentonit verfüllt werden. In den Richtlinien der Behörden wird für den Lagerbehälter eine Auslegung für einen Einschluss der Radionuklide während 1'000 Jahre verlangt, von der Nagra angestrebt wird jedoch ein Einschluss während mehr als 10'000 Jahren. Das Porenwasser, mit dem die Behälter umgeben sind, ist marinen Ursprungs mit etwa 0.1-0.3 M Cl^-. Weil durch die Korrosion Wasserstoff gebildet wird, ist eine Abschätzung der Wahrscheinlichkeit von Wasserstoff-induzierter Rissbildung und die Erarbeitung von Empfehlungen, wie eine solche verhindert werden kann, erforderlich.

Deshalb wurden die wichtigsten Berichte evaluiert, die bezüglich der lokalen Bedingungen und den dort erwarteten Korrosionsraten der Lagerbehälter von Relevanz sind, im Hinblick auf die Beurteilung der Auswirkungen der im Stahl vorhandenen Wasserstoffkonzentration. Einfache Berechnungen der Diffusion und Akkumulation von Wasserstoff im Inneren des verschweissten Behälters zeigen, dass in der zu betrachtenden Zeit ein Gasdruck erreicht wird, der mit dem vom Gas ausserhalb des Behälters vergleichbar ist (ca. 10 MPa). Dies ist wichtig, weil die innere Oberfläche der Schweissnaht, die beim Verschluss des Behälters entstanden ist, nicht bearbeitet werden kann. Im vorliegenden Bericht werden die heute vorhandenen Kenntnisse zu Mechanismen zur Wasserstoff-induzierten Rissbildung diskutiert. Die Diskussion ergibt, dass das mechanistische Verständnis und die entsprechenden Modelle für Wasserstoff-induzierte Rissbildung keine quantitative Voraussage solcher Phänomene erlauben. Deshalb beschränkt sich der Bericht auf die Identifikation und Festlegung von Grenzwerten und Bedingungen bezüglich Rissbildung und auf eine Abschätzung der Wahrscheinlichkeit, dass diese Grenzwerte und Bedingungen innerhalb der Lebensdauer des Behälters überschritten werden könnten. Basierend auf einer Analyse der Daten wird eine Rissbildung als sehr unwahrscheinlich eingeschätzt. Im Bericht werden Empfehlungen gemacht zur Auswahl der Stahlzusammensetzung, der Stahlbearbeitung und der Schweissverfahren, damit die Möglichkeit der Rissbildung für den Endlagerbehälter für die erwarteten Lagerbedingungen praktisch ausgeschlossen werden kann.

Résumé

En Suisse, la Société coopérative nationale pour le stockage des déchets radioactifs (Nagra) est chargée de développer une méthode efficace pour le stockage sûr des déchets de haute activité vitrifiés (DHA) et des assemblages combustibles usés (AC). Parmi les matériaux envisagés pour les conteneurs de stockage figure l'acier au carbone. Ces conteneurs à parois épaisses, d'un diamètre d'environ 1 m et d'une longueur d'environ 3 m (DHA) ou d'environ 5 m (AC) seront placés dans des galeries horizontales et entourés d'un remplissage de bentonite. Les directives de l'autorité de sûreté exigent que les conteneurs assurent le confinement des radionucléides sur une durée de 1000 ans, mais la Nagra souhaite garantir cette fonction sur plus de 10.000 ans. L'eau interstitielle dans l'environnement des conteneurs est d'origine marine avec 0.1-0.3 M Cl^-. En raison de la présence d'hydrogène résultant des réactions de corrosion, il est nécessaire d'estimer la probabilité d'une fissuration assistée par l'hydrogène et d'effectuer des recommandations sur les mesures à prendre pour éliminer cette probabilité.

Dans cette perspective, on a analysé les principaux rapports détaillant l'évolution du milieu ambiant et les taux de corrosion qui en résultent pour les conteneurs de stockage, en étudiant particulièrement les conséquences du processus sur la concentration d'hydrogène absorbé par l'acier. Des calculs simples portant sur la diffusion et l'accumulation d'hydrogène dans le compartiment interne du conteneur scellé indiquent que la pression atteinte au cours de la période considérée équivaut à celle du gaz présent à l'extérieur du conteneur (estimée à environ 10 MPa). Ceci est une donnée importante, car il n'est pas possible de traiter la surface interne de la soudure effectuée lors du scellement du conteneur. Les théories actuelles relatives à la fissuration assistée par l'hydrogène ont été passées en revue. Il en ressort que les phénomènes mécaniques et les modèles correspondants ne sont pas suffisamment maîtrisés pour autoriser des prédictions quantitatives dans le cadre de l'application envisagée. Dès lors, le présent rapport se borne à identifier les conditions et valeurs limites prévalant lors de la fissuration et d'estimer la probabilité selon laquelle ces conditions et valeurs limites pourraient être dépassées au cours de la durée de vie du conteneur. L’analyse de ces données permet de conclure qu’une fissuration est extrêmement improbable. Ce rapport fournit des recommandations quant au choix de la composition de l'acier, de son traitement et des procédés de soudure, afin d'éliminer autant que possible la probabilité de fissuration dans le cadre des conditions présumées pour le conteneur de stockage.

Table of Contents

Abstract I
Zusammenfassung II
Résumé III
Table of Contents V
List of Tables VI
List of Figures VII
List of Abbreviations VIII

1 Introduction 1

2 Description of the near field conditions 3
2.1 The local environment external to canister 3
2.2 Environment inside canister 5
2.3 Corrosion and hydrogen generation 6
2.4 Summary of Section 2 12

3 Hydrogen uptake and transport 13
3.1 Trapping in carbon steels 13
3.2 Estimation of C_0 values 14
3.3 Diffusion and the time evolution of hydrogen in the canister wall 18
3.3.1 Diffusion coefficients 18
3.3.2 Modelling the internal pressure build-up and the hydrogen distribution in the canister wall 20
3.4 Summary of Section 3 23

4 Review of hydrogen related degradation mechanisms for C-steel 25
4.1 Hydrogen-induced cracking (HIC) and stress oriented hydrogen - induced cracking (SOHIC) 25
4.2 Hydrogen enhanced decohesion (HEDE) 27
4.3 Adsorption induced dislocation emission (AIDE) 27
4.4 Hydrogen-enhanced local plasticity (HELP) 28
4.5 Summary of Section 4 28

5 Threshold conditions for cracking 29
5.1 Threshold stress intensity factor 30
5.2 Threshold conditions for hydrogen-induced cracking (HIC) and stress-oriented hydrogen-induced cracking (SOHIC) 34
5.2.1 Threshold hydrogen concentration for hydrogen-induced cracking 34

5.2.2 Threshold hydrogen concentration for stress oriented hydrogen-induced cracking 35
5.2.3 Threshold temperature for hydrogen-induced cracking..... 36
5.2.4 Effect of steel composition on hydrogen-induced cracking 36
5.2.5 Effect of microstructure on hydrogen-induced cracking and stress oriented hydrogen-induced cracking 37
5.2.6 Effect of mechanical properties on hydrogen-induced cracking 38
5.2.7 Effect of weldments on hydrogen-induced cracking and stress oriented hydrogen-induced cracking 38
5.3 Summary of Section 5 39

6 Summarised assessment of the potential for cracking 41

7 Mitigation strategies to minimise likelihood of cracking associated with hydrogen 43

8 Concluding remarks 45

9 References 47

APPENDIX – Approximate calculation of hydrogen pressure build up inside canister
1 Diffusion through a flat plate..... 1
2 Application to the practical problem 2

List of Tables

Tab. 1: Pore water composition and evolution (M) (Curti & Wersin 2002). 3
Tab. 2: Estimated lattice hydrogen content (C_0) for different exposure conditions. 15
Tab. 3: Approximate estimates of time evolution of pressure at 90 °C, assuming zero concentration boundary condition at inner surface, a value of 0.03 ppm (2.37×10^{-7} moles/cm^3) at the outer surface and a 15 cm thick canister wall. 22
Tab. 4: K_{th} for different strength steels as function of hydrogen fugacity at room temperature (San Marchi et al. 2008). 32

List of Figures

Fig. 1: Simulated evolution with time of temperature and relative humidity at the surface of a spent fuel canister at different locations with respect to the cross-section center (data provided to CMRB by Nagra, based on Senger & Ewing 2008). 4

Fig. 2: Relationship between potential hydrogen and weld hydrogen (after Coe 1973). 6

Fig. 3: Summary of the anaerobic corrosion behaviour of C-steel in bulk solution and in compacted clay (after Johnson & King 2008). 8

Fig. 4: Corrosion rate in Äspö groundwater at 85 °C (after Smart et al. 2002a). 9

Fig. 5: Compilation of anaerobic corrosion rates for carbon steel in current Nagra canister lifetime prediction (after Johnson & King 2008). 10

Fig. 6: Impact of sulphide addition on hydrogen permeation current for a linepipe steel exposed to trapped ground-water (Cheng et al. 2000). 16

Fig. 7: Compilation of diffusion data (after Boellinghaus et al. 1995). 19

Fig. 8: Schematic of sulphide stress cracking (SSC), SOHIC and HIC processes (after Christensen 1999). Type I is considered to represent failure in high strength steels and Type II to represent failure in medium and low strength steels in what was later termed SOHIC. Blistering is associated only with very severe charging in acidic H_2S environments and is not applicable to this waste containment application. 26

Fig. 9: Schematic illustration of the zones of susceptibility of carbon steel to hydrogen related degradation mechanisms (JNC 2000). 29

Fig. 10: Modified Kitigawa-Takahashi plot showing the threshold stress for stress corrosion cracking as a function of crack size. 30

Fig. 11: Lower-bound trends drawn to represent the results of over 400 measurements of the threshold stress intensity factor for internal and external hydrogen assisted cracking at 23 °C (after Gangloff 2003). 31

Fig. 12: Temperature dependence of K_{th} for 4340 steel in hydrogen gas (after San Marchi & Somerday 2008). 32

Fig. 13: Variation of the pitting factor with the average depth of corrosion derived form long-term corrosion tests and short-term laboratory measurements (from Johnson & King 2008, based on JNC 2000). 33

Fig. 14: Critical hydrogen permeation coefficient (a) and Crack Area ratio (b) as a function of hardness in simulated segregation zone (after Takeuchi et al. 2004 *cited in Herrmann et al. 2005*). 35

Fig. 15: HIC susceptibility defined by hardness of segregation areas in relation to relative amounts of P and Mn (Li et al. 1966 and Toyama & Konda 1989). 37

List of Abbreviations

AIDE	adsorption-induced dislocation emission
AISI	American Iron and Steel Institute
HAZ	heat-affected zone
HEDE	hydrogen-enhanced decohesion
HELP	hydrogen-enhanced localized plasticity
HIC	hydrogen-induced cracking
SOHIC	stress oriented hydrogen-induced cracking
SSC	sulphide stress cracking

1 Introduction

The long-term disposal of high level nuclear waste can be achieved by a number of routes, all of which involve deep geological repositories chosen to provide an inherent natural barrier minimising ground water migration. The geological constituents of the considered sites vary and include tuff, granite, clay, and rock salt. In addition to variation in local geology, different approaches to the material of containment and the surrounding local environment are also being considered (Féron & Macdonald 2003). In the Yucca Mountain project in Nevada, the approach proposed has been to install the canisters in an excavated cavern with the effective exposure conditions being a relatively humid atmosphere and deposits formed on the metal surface as dust particles from the surrounding rock (Féron & Macdonald 2003). A titanium drip shield would limit direct dripping of water onto the canisters. The focus then is on adopting highly corrosion resistant alloys (Alloy C-22 is proposed) such that corrosion or stress corrosion cracking is either extremely unlikely or propagates sufficiently slowly within the required timeframe. The alternative approach, more commonly being considered, involves adoption of less corrosion resistant alloys but configuring the environment immediately surrounding the canisters to progressively become of such low aggressivity that any corrosion mode initiated can be tolerated over the proposed disposal period.

In Switzerland, the National Cooperative for the Disposal of Radioactive Waste (Nagra) is responsible for establishing an effective method for safe disposal of vitrified high level waste (HLW) and spent fuel. One of the options for disposal canisters is thick-walled carbon steel. The canisters, which should have a diameter of about 1 m and length about 3 m (HLW) or about 5 m (spent fuel), will be embedded in horizontal tunnels and surrounded in the immediate environment with bentonite clay (Johnson & King 2003 and 2008). The regulatory requirement for the minimum canister lifetime is 1'000 years but demonstration of viability over 10'000 years would be desirable. The adoption of a low strength carbon steel would appear unusual at first as it not intrinsically a corrosion resistant alloy and the pore water will have marine origins. However, it is less likely to experience severe localised corrosion, compared with a corrosion resistant alloy, over any timescale of significance. There is then arguably greater confidence in prediction of long-term corrosion rates and in estimating the required thickness of the canister. Although oxygen would be introduced during installation this would be consumed with time, as there is negligible replenishment, and the period of aeration is relatively short. Microbial activity is also not feasible so that the only long-term driving force for corrosion is water reduction (Johnson & King 2003 and 2008). The other advantages of using carbon steel are relative ease and flexibility of fabrication, extensive history of usage in diverse applications, and relatively low cost.

Whilst general corrosion and localised corrosion, insofar as it is relevant, can be accounted for with some degree of confidence there is a need to show also that environment induced cracking modes are not sustainable. Nominal stresses (about 30 MPa maximum) will be very low compared to the yield stress (projected to be about 235 MPa, see Johnson & King 2003) but the sealing caps will be welded without the benefit of stress relief (the required temperature would affect the fuel/vitrified waste). The lack of stress relief would lead to the possibility of stresses near yield, though this could be the yield strength associated with the local microstructure in the heat-affected zone (HAZ) and not simply the parent steel. While grinding of the cap may be feasible, this is intrinsically not possible for the weld root. There is no dynamic loading on the canisters that might induce a fatigue component. However, hydrogen atoms are generated in the cathodic reduction of water. Some will enter the steel and progressively diffuse through to the inner chamber of the canister but most of the hydrogen atoms generated will recombine to form molecular hydrogen in solution. In most applications this dissolved molecular hydrogen diffuses

away and no longer impacts on hydrogen uptake. However, in this repository, transport in the bentonite and Opalinus Clay is highly restricted leading to the dissolved molecular hydrogen concentration exceeding the solubility limit and precipitating in the pores in the bentonite as gaseous hydrogen. Calculations (Johnson & King 2003) suggest that the partial pressure may approach 10 MPa*. A gas interface with the external canister surface then provides an alternate process for hydrogen uptake.

Thus, there will be combination of stress and absorbed hydrogen atoms from either direct electrochemical reduction of water or from dissociation of molecular hydrogen adsorbed on the surface from the gas phase. The purpose of this review is to assess the implications for integrity of the carbon steel canisters and to identify mitigation strategies that would ensure that any risk is minimised.

* It was not within the scope of this review to evaluate the reliability of this partial pressure calculation.

2 Description of the near field conditions

2.1 The local environment external to canister

The repository for locating the canisters is planned to be excavated in Opalinus Clay with the important characteristic that transport in the clay is diffusion controlled, ruling out any flow-assisted transport of potential reactant species (see Johnson & King 2003 for detailed background). The clay is also self-sealing so that fractures are expected to be transient. The canisters will sit on bentonite blocks and the region around the canisters will be back-filled with granular bentonite. The blocks will tend to have a higher moisture content than the granular bentonite, with an initial moisture content of 15 % for the blocks projected. After sealing there is a partial pressure differential of about 6 MPa that will drive water from the Opalinus Clay to the bentonite and thus eventually to the canister with hydration of cations acting as a kind of suction force drawing water into the clay structure. The uptake of water causes swelling of the clay, thus forming tight contact with the canister and the rock and inducing a self-sealing capability with respect to voids or cracks. Ion diffusivity will also be low.

The pore-water to which the canister will be exposed will have marine origins with about 0.1-0.3 M Cl^- and a nominal pH in the region of 6.9-7.9 (at 25 °C). The projected water chemistry of the pores is listed in Tab. 1 (Curti & Wersin 2002).

Tab. 1: Pore water composition and evolution (M) (Curti & Wersin 2002).

			Maximum expected variation	
	Opalinus Clay	**Bentonite reference water**	**Bentonite low pH**	**Bentonite high pH**
pH	7.24	7.25	6.9	7.89
log pCO_2 (bar)	-2.2	-2.2	-1.5	-3.5
Ionic strength (eq/l)	2.28×10^{-1}	3.23×10^{-1}	3.65×10^{-1}	2.63×10^{-1}
CO_3	2.70×10^{-3}	2.83×10^{-3}	6.99×10^{-3}	5.86×10^{-4}
Na	1.69×10^{-1}	2.74×10^{-1}	2.91×10^{-1}	2.49×10^{-1}
Ca	1.05×10^{-2}	1.32×10^{-2}	1.33×10^{-2}	1.34×10^{-2}
Mg	7.48×10^{-3}	7.64×10^{-3}	8.91×10^{-3}	6.15×10^{-3}
K	5.65×10^{-3}	1.55×10^{-3}	1.67×10^{-3}	1.38×10^{-3}
SO_4	2.40×10^{-2}	6.16×10^{-2}	6.39×10^{-2}	5.59×10^{-2}
Cl	1.60×10^{-1}	1.66×10^{-1}	2.06×10^{-1}	8.61×10^{-2}
Fe	4.33×10^{-5}	4.33×10^{-5}	7.74×10^{-5}	8.00×10^{-6}
Al	2.17×10^{-8}	1.92×10^{-8}	1.53×10^{-8}	7.55×10^{-8}
Si	1.78×10^{-4}	1.80×10^{-4}	1.80×10^{-4}	1.84×10^{-4}

The temperature distribution around the canister will be variable because of the additional moisture in the bentonite block support (and associated higher thermal conductivity) though model calculations of the time evolution of the distribution have been made. It is suggested that the temperature at the canister will rise progressively over 10 years to about 120 °C before decaying (Senger & Ewing 2008; see Fig. 1).

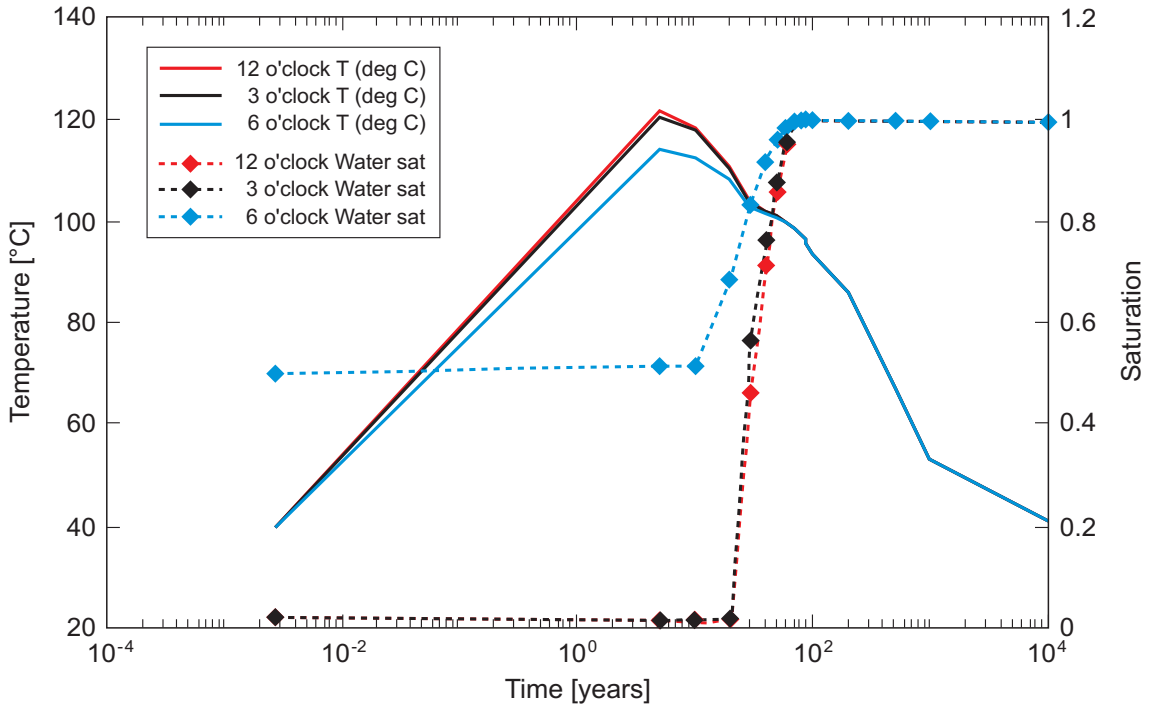

Fig. 1: Simulated evolution with time of temperature and relative humidity at the surface of a spent fuel canister at different locations with respect to the cross-section center (data provided to Canister Materials Review Board (Landolt et al. 2009) by Nagra, based on Senger & Ewing 2008).

The distribution of water will be complex with the environment around the canister being essentially hot moist air in the initial high temperature phase (no condensation at this stage) but an evaporation front will develop that will progressively move to the canister as the temperature decays (accelerating the latter process as it does so). However, the evaporation front might be expected to vary round the canister in a complex way because the initial water content of the bentonite blocks is higher than that of the pellets, prompting a migration of water from the block to the pellets. As the chloride content of the pore water in the backfill will lie between 0.1 M and 0.3 M, with additional calcium salts from the bentonite a salt layer could develop at the leading edge of the evaporation front. When this is remote from the canister, this is not an issue; it progressively dissolves as the liquid front advances. However, as the temperature of the canister decreases the gradient in water content due to the block may result in an evaporation front that attains a stable liquid face preferentially close to the bentonite blocks. This will be affected by the initial moisture and chloride content of the blocks and the extent to which water in the blocks is driven to the backfill. Modelling of the evolution of the water saturation level (Fig. 1) does indicate that the moisture content close to the bentonite block will be somewhat higher but the time at 100 % saturation, at which a liquid phase is formed, is predicted to be fairly similar at different locations around the canister. However, the effect of salts and of capillary condensation at the base of the canister should not be overlooked.

An evaporation front would create a three-phase boundary between the gas phase containing oxygen, the metal and the water phase with a salt deposit at the leading edge. It might be expected that the solution at the evaporation front might be rich in Mg salts but for complex media prediction is not straightforward (Turnbull et al. 2008). Such local salt conditions can arise also from deliquescence of impurities (Johnson & King 2008), from the bentonite, e.g. halite (NaCl) and gypsum ($CaSO_4.2H_2O$), or from handling and transport of the canisters. The effect of these particles will be to encourage formation of droplets in local regions, an associated concentrated salt solution, and localised corrosion because of the ready supply of oxygen.

The oxygen concentration in the gas phase will initially be that of air with an equilibrium concentration in the liquid determined by the local temperature. Gettering of the oxygen will occur by corrosion of the canisters and the carbon steel mesh used as a rock support and by oxidation of pyrite. The latter may generate sulphur species such as HS^- ions, possibly oxidised to thiosulphate during the aerated phase, as suggested by Johnson & King (2008) though they do not indicate the predicted concentration at the metal surface and the supply kinetics during the transient phase when corrosion is non-uniform. Nevertheless, given the restricted transport and active corrosion of the canister it would be assumed reasonably that the sulphide species would be consumed at their transport-limited rate. Thermodynamically (Pourbaix 1996), reduction of sulphate ions to HS^- ions could occur when the potential decreases in response to depletion of oxygen. It is generally assumed that the kinetics at the canister temperature are too sluggish (JNC 2000) to influence the total cathodic current (though locating specific data for electrochemical reduction kinetics has not been possible despite the relative simplicity of the experiments). It is not a trivial issue as even a slow reaction in a constrained environment can eventually affect the nature of the surface film. Reduction of sulphate via sulphate reducing bacteria will be inherently determined by microbial activity but such activity is considered to be very limited (Johnson & King 2008).

In principle, radiolysis could be a source of oxidising species but the wall thickness (projected to be 15 cm) proposed for the canister steel for ready handling and also for corrosion resistance will be such as to render this insignificant.

2.2 Environment inside canister

The canister will be sealed in air with a relative humidity and oxygen concentration reflecting the local conditions at the time of closure. Inside the canister, with a projected free volume of about 0.15 m^3*, the hydrogen partial pressure will rise progressively with time as hydrogen generated on the external surface diffuses through the canister wall. Correspondingly, the dissolved hydrogen concentration at the internal surface will increase. The time evolution of this is an important consideration as there is no possibility of modifying the surface state of the root of the closure weld, which could contain local defects, together with residual stress. Retained oxygen in the cavity might at first sight appear to inhibit the likely sensitivity to cracking (Murray 1988) but this is less relevant in a situation where hydrogen is fed to the internal cavity via the canister walls, for which the primary effect of the build-up of internal pressure is to reduce the hydrogen concentration gradient in the steel. Some additional contribution to the internal hydrogen may come from hydrogen introduced during the welding. This will diffuse to the internal chamber as well as to the external environment. However, the magnitude of the contribution to the pressure is probably modest assuming a fillet weld as a simple cap-sealing weld with a relatively small amount of weld metal. Gas-shielded metal arc welding should minimise the amount put into the steel (Coe 1973), as shown in Fig. 2.

* The exact value will depend on the detailed design but is likely to be of this order.

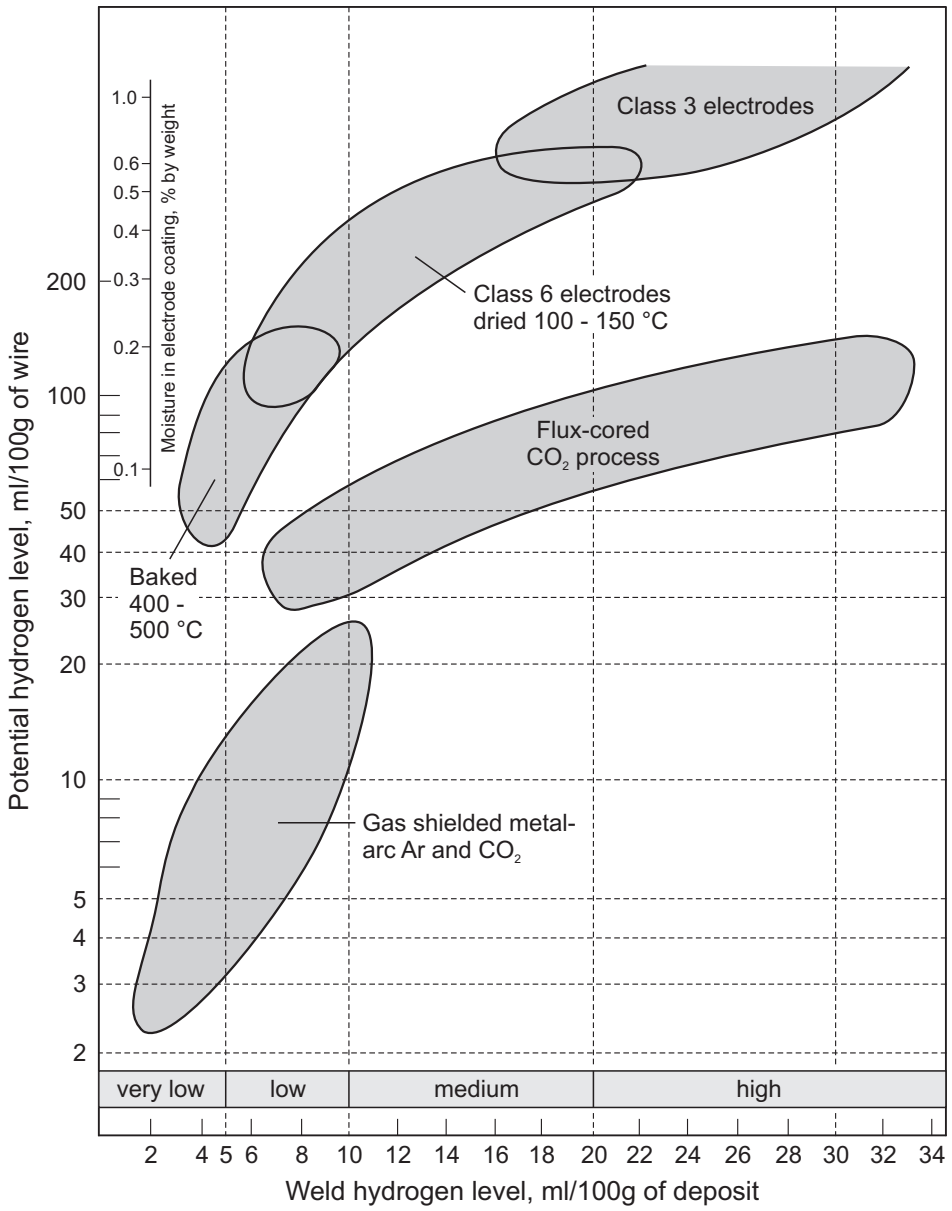

Fig. 2: Relationship between potential hydrogen and weld hydrogen (after Coe 1973).

2.3 Corrosion and hydrogen generation

As described by Johnson & King (2008) there are different stages of corrosion, reflecting the change in environmental exposure conditions with time:

- initial hot moist atmosphere but no wetting of the canister
- aerated conditions in which a three-phase boundary will exist
- aerated but fully wetted conditions for a period until oxygen is depleted
- transient period where reduction of higher oxides formed during the aerated phase provides a cathodic reaction process, slowing the decay in potential despite oxygen depletion
- anaerobic phase where reduction of water is the dominant cathodic reaction

Johnson and King surmise a high potential (about -0.05 V SCE) during the initial aerated phase which is a little unexpected for the concentrated solution that may develop and would be inconsistent with the observation of active corrosion, albeit in fully immersed conditions, noted by Taniguchi et al. (1998). Relatively noble potentials of about -0.2 V SCE, not as high as envisaged by Johnson & King (2008) and not representing passivity, can arise in some dilute chloride conditions (1.5 ppm) at the relevant temperature if the dissolution rate becomes limited by build up of corrosion products and metal ion diffusion is restricted (Turnbull & Zhou 2004) but this seems unlikely for these relatively concentrated solutions. It is also unclear to what extent reaction with sulphur species transiently drives the corrosion potential.

The corrosion rate will be most significant near the leading edge if an evaporation front interfaces with the canister and at droplets formed around salt impurities. Corrosion at a water-line and at droplets is known to be more intense partly because of high concentration of salts at a three-phase boundary (though buffering from the bentonite should preclude the decrease in pH associated with concentrated salts) but with a possible contribution from surface tension driven flow (Marangoni effect, see http://en.wikipedia.org/wiki/Marangoni_effect) and thus enhanced local transport of dissolved oxygen. However, progressively the three-phase boundary will dissipate as the surface becomes uniformly wetted and dilution of salts occurs. However, local pitting regions might retain some chloride whilst some oxidant is present. Predicting the local pH under such conditions is quite complex because ferric ion formation from oxidation of ferrous ions could give quite acidic conditions at local anodes (though at the mouth of pits rather than the base), whilst at the cathode the pH will be elevated. Counterbalancing these pH changes will be buffering by the bentonite clay.

Analysis of the role of sulphur species is challenging. There will be a transitory phase where the presence of oxygen may create high oxidation states such as thiosulphate and enhanced corrosion should ensue (Johnson & King 2003). At longer times, there will be transport of sulphides to the canister from the pyrite but at a very slow rate. More information on the time-evolution of the local concentration and supply kinetics and the impact on surface films would be enlightening. As noted in the previous section it might be expected that the corrosion rate would quickly become supply limited with a very low flux. Johnson & King (2008) suggest that over 10'000 years sulphide-induced corrosion amounts to only about 0.2 mm of material loss. This figure supersedes the 9 mm over 1'000 years reported previously (Johnson & King 2003). There has been no accounting for the direct electrochemical reduction of sulphate to HS^- ions as noted in Section 2.2 and some experimental evaluation is merited. In relation to sulphur species in solution and sulphide stress cracking the oil and gas community standard, ISO 15156-2 (2003), classifies the environment as non-sour when the partial pressure of H_2S is less than about 0.3 kPa (an equivalent concentration in solution of about 10 ppm at ambient temperature). In this context non-sour means that only particularly susceptible alloys would be likely to crack. There is no basis for considering that the local concentration in the water surrounding the canister could contain 10 ppm H_2S on a sustained basis and even in the short term when corrosion may be localised it seems very unlikely. At longer times, uniform corrosion would consume sulphide species more effectively and the rate of replenishment would be very low.

At sufficiently long times, towards 100 years, the temperature will drop sufficiently that there will be a continuous liquid phase at the canister with a salt concentration in the pores at the bulk value. The oxygen will have been consumed at this time and the corrosion will be driven only by the water reduction kinetics.

From the viewpoint of electrochemical generation of hydrogen the greatest challenge is predicting the evolution of the hydrogen distribution in the steel between 10 and 100 years when there is a period of non-uniform wetting of the surface and where corrosion is non-uniform. It seems unlikely that the corrosion potential will be very noble at the three-phase boundary as

film stability in a concentrated solution would be poor. Localised corrosion is likely. Predicting the extent of hydrogen generation is a challenge. The potential in a pit will be limited to an extent by IR drop but may be sufficiently positive to lead to a fall in local pH. The magnitude of the pH in a pit in carbon steel (with no Cr) at this temperature is hard to predict. At ambient temperature, the lowest pH would be about 4 (assuming deaeration at the pit base and a concentrated $FeCl_2$ solution; see Turnbull 1983) but reliable measurement and modelling for elevated temperatures of about 100 °C under these conditions has not been conducted. The closest comparison perhaps is cracks in steam turbine disc steels (Turnbull & Zhou 2001) for which a pH of between 5 and 6 was predicted under some circumstances but here the bulk solution was much more dilute. As noted above, an acid pH just outside the pit is possible because of oxidation of ferrous ions to ferric by reaction with oxygen in the water. This may enhance pit mouth broadening. However, it may be argued that buffering by the bentonite clay may constrain such a drop in pH. The key point is that the more noble potential during the oxygen phase does not mean that the kinetics of hydrogen generation can be neglected; it just implies that where it may be significant it will be localised and associated with locally low pH values. At long times, when oxygen is depleted, it is expected that a stable film will persist on the surface, that water reduction will be the source of hydrogen atoms and the kinetics will be slow.

The nature of the film in compacted clay is suggested to be a complex Fe, Ca-containing carbonate film (Fig. 3).

	Bulk solution	**Compacted bentonite**
Corrosion rate and time dependence	~ 0.1 μm ·yr^{-1} Steady-state after 4-6 months e.g., Smart et al. (2001), Kreis and Simpson (1992)	~ 1 μm ·yr^{-1} Still decreasing after 4 yrs e.g., Taniguchi et al. (2004), Papillon et al. (2003)
Corrosion products: composition and structure	Duplex spinel-type/Fe_3O_4 structure 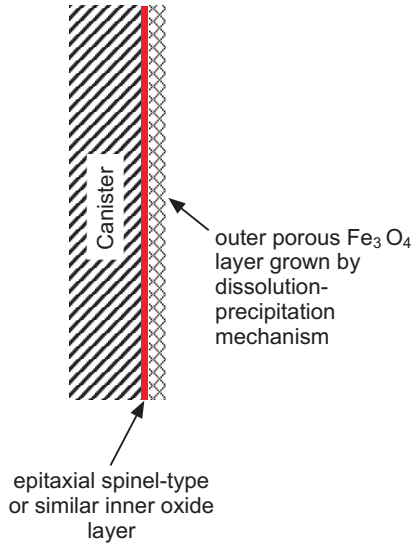	Thick $FeCO_3$/(Fe, Ca) CO_3-containing dense product layer and adjoining altered soil layer 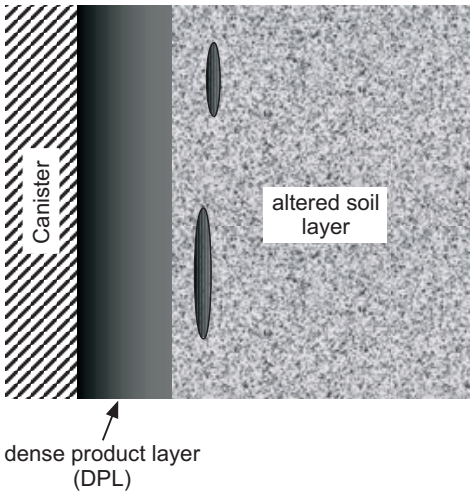

Fig. 3: Summary of the anaerobic corrosion behaviour of C-steel in bulk solution and in compacted clay (after Johnson & King 2008).

Note that recent ideas on CO_2 corrosion in the oil and gas industry (Han et al. 2008) suggest a thin passive oxide film beneath the carbonate layer with the latter acting as a diffusion barrier allowing the pH to rise and stabilising the magnetite film*. There appears to be no indication of such an oxide here under anaerobic conditions. However, as noted by Johnson & King (2003 and 2008) complex oxides would be expected to form during the transitory period of exposure to oxygen with some reduction of higher oxidation state occurring at later times. This perception of the surface film was based on measurements in a sulphide-free environment. The possible extent of FeS or more complex sulphide films is unknown, noting that even very slow reactions involving sulphur species could affect the film characteristics. Nevertheless, the long-term corrosion rate is projected to be very low indeed and for compacted clay about 1 μm/y (approximately 0.1 μA/cm^2). Hence, a very low charging current density will prevail at long times. This long-term corrosion rate is based on the work of Smart et al. (2002a and b) and other authors (review by King & Stroes-Gascoyne 2000) as summarised in Figs. 4 and 5. In the former, the surface film was magnetite (cf. Fig. 3).

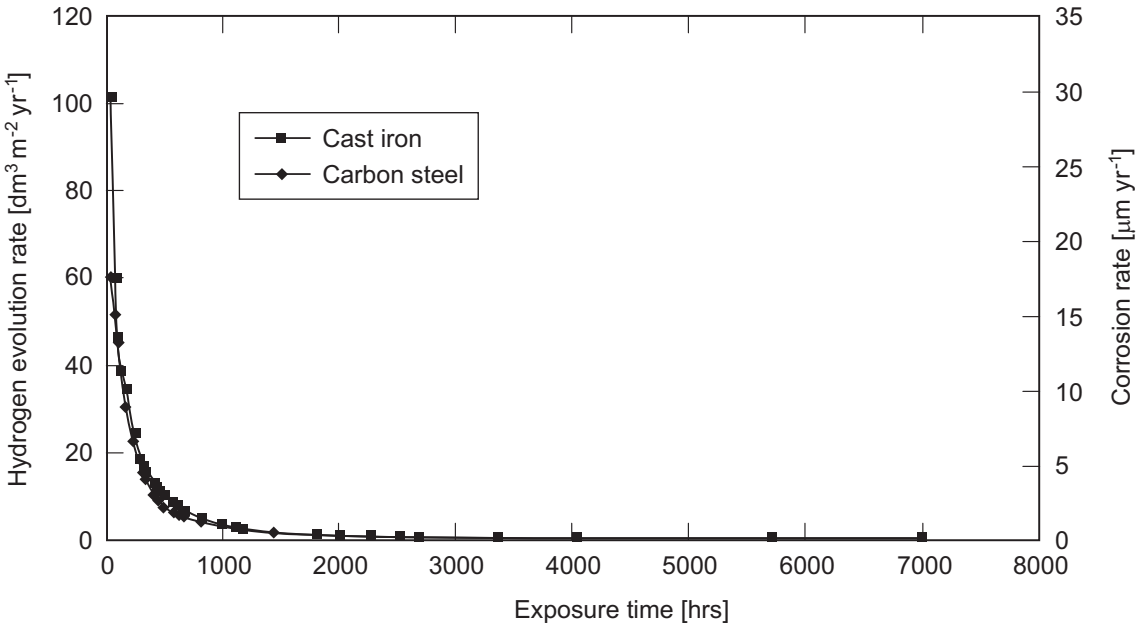

Fig. 4: Corrosion rate in Äspö groundwater at 85 °C (after Smart et al. 2002a).

* Although Han et al. (2008) refer to a $Fe(OH)_2$ film at 80 °C the most likely film at this temperature is magnetite.

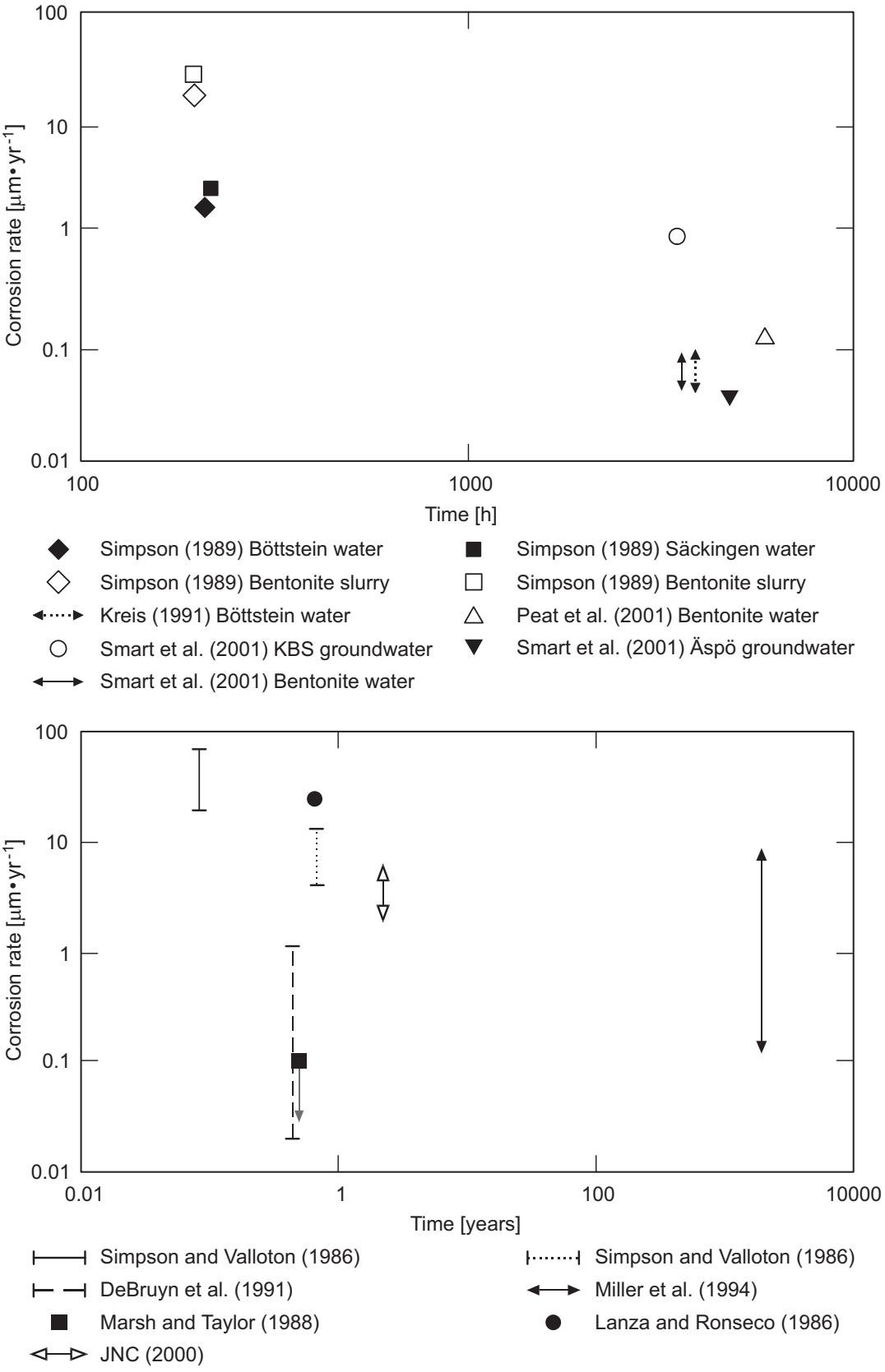

Fig. 5: Compilation of anaerobic corrosion rates for carbon steel in current Nagra canister lifetime prediction (after Johnson & King 2008).

A key feature of this repository is the extremely low transport rate of species through the clay. As a consequence, reaction product dispersion will be poor and this will include molecular hydrogen. The concentration of molecular hydrogen in solution will build up and eventually precipitate as a gas phase. Gas phase transport is itself also significantly restricted and so gas pockets may develop with pressures estimated at 10 MPa (see Johnson & King 2003) though such pressures may take a few hundred years to establish. It is likely that there will be an interface between the gas phase and the canister at some location.

It might be expected that with restricted removal of the cathodic reaction products then corrosion rates would fall to the transport limited rate determined by the rate of hydrogen loss through the pores of the clay and rock and also into the steel. Smart et al. (2002a and b) claimed that there was no difference in corrosion rate even with high pressures of hydrogen gas. The raw data did not seem to support that conclusion, suggesting the corrosion rate was higher at higher pressure (contrary to expectations), although Smart et al. argue that the results were within experimental error. They essentially conclude that the corrosion rate was anodically controlled and restricted by cation transport through the magnetite film (in this study, the pH was somewhat higher than for the Nagra pore water chemistry). They claim that there is no effect of hydrogen pressure on the corrosion potential. However, this appears to be based on relatively short-term tests and would imply that the dissolution rate was significantly higher than the hydrogen oxidation rate. At first sight, it would be surprising if this were the case at very long times for which a very low dissolution rate is expected and the dissolved hydrogen gas content in equilibrium with 10 MPa should be relatively high. Intuitively, it would seem more likely that the system would be close to the reversible electrode potential for the hydrogen electrode with corrosion limited only by the rate of removal of hydrogen atoms, through diffusion in the steel and recombination and diffusion in solution with the former relatively enhanced because of restricted transport in the latter case. However, it is feasible that the efficiency of hydrogen oxidation on the surface would reduce with time and, thus, the contribution to the total oxidation current would be small.

An intriguing issue is whether separation of anodes and cathodes in a redox system could occur because of variation in effective mass transfer and non-uniformity of reaction.

Oxidation of hydrogen is referred to above as possibly affecting the mixed potential. However, absorbed hydrogen is known also to affect the stability of oxide films leading to enhanced corrosion and reduced pitting corrosion resistance. Much of that research has focused on corrosion resistant alloys, often in severe pre-charging conditions (see Hasegawa & Osawa 1980 as example) and without reference to the absorbed hydrogen content. There is evidence to support a similar effect of absorbed hydrogen on corrosion of iron where the passive film has been formed in borate solution but no information about the absorbed hydrogen concentration was given (Yu et al. 2001). Again the system was pre-charged. It is less clear that such a process will affect the waste containers as it presumes that some form of protective oxide will prevail on the canister surface. It is also not clarified whether the effect will be seen with a magnetite film. In any case, any effect, should it exist, will be confined to relatively short exposure times. At long times the steel will tend to corrode in the active state.

2.4 Summary of Section 2

- Hydrogen generation kinetics will be most significant during the transient aerated period but will diminish at long times.
- During the transient period, the corrosion rate will be most pronounced where there is a three-phase boundary, at droplets and at an evaporation front if wetting of the canister is non-uniform.
- At longer times as the gradient in hydrogen concentration though the pore solution diminishes slow transport of molecular hydrogen away from the canister surface may lead to a higher concentration of adsorbed hydrogen atoms and encourage hydrogen uptake (assuming that the corrosion rate is not intrinsically slower than the rate of transport of molecular hydrogen which must eventually be the case when the buffer is fully saturated).
- The concentration of sulphide species in the local environment at the canister surface is not ideally characterised in terms of the impact on short-term hydrogen update but there is no significant sustainable supply of sulphide species to maintain a significant hydrogen flux. The environment would tend to be classified as non-sour.

3 Hydrogen uptake and transport

The corrosion process, generating hydrogen electrochemically, and exposure to hydrogen gas determine the lattice concentration sub-surface (C_0) as a function of time and temperature. The sub-surface lattice concentration is the baseline parameter that feeds into calculation of the hydrogen profile with time, using appropriate diffusivity data, and is the reference value that limits the localisation associated with traps and local stress. Hydrogen in the steel will be distributed between lattice and microstructural trap sites with the greatest concentration in the latter for the modest temperatures associated with the repository conditions. Here we will describe trapping in the steel from the viewpoint of diffusivity, focus then on lattice hydrogen, and finally discuss diffusivity data and hydrogen build-up.

3.1 Trapping in carbon steels

Trapping of hydrogen will occur at microstructural sites because the potential well for the trap site is deeper than for the interstitial lattice site, causing the hydrogen atom (strictly speaking it is the proton but we will refer throughout to the atom) to sit in the site for longer than the lattice site. For very deep potential wells there is effectively zero probability of the hydrogen jumping out of the trap site at the temperature of interest and these are referred to as irreversible trap sites. In general, these deeper trap sites tend to be filled with hydrogen during processing and then have little influence on diffusivity, although there are exceptions. If the fluctuations in thermal energy are such as to enable the hydrogen atom to jump out of a trap site then these are referred to as reversible trap sites. It should be emphasised that there is no strict cut-off in terms of a binding energy that separates reversible traps from irreversible traps, essentially the probability of an atom jumping out of a trap simply gets smaller and smaller with increase in binding energy to the point that it becomes insignificant. Clearly, the probability will increase with temperature, the residence time will decrease, and the effective diffusivity will increase.

There is a plethora of trapping sites in steel, including grain boundaries, phase boundaries, dislocations, interfaces between the matrix and inclusions and particles, vacancies and solute atoms. Voids formed at interfaces can also be classified as traps but with the distinction that these are dynamic traps (often described as non-saturable, see Johnson 1988) as they increase their capacity in response to progressive hydrogen uptake. The significance of the different trap sites for diffusion depends on the density and binding energy and in the case of voids, whether the threshold hydrogen content for void growth has been exceeded. In the latter case, it is not readily possible to assign an effective diffusivity. In permeation experiments, the growth of voids should cause a peak in the flux vs time relationship as the effective trap density (trap volume in this case) is increasing with time. There are parallels here with the critical concentration of hydrogen for hydrogen-induced cracking (HIC) in H_2S environments but there are complications in many of the traditional permeation studies in H_2S environments because film formation can retard hydrogen uptake and also cause a peak in permeation flux. Permeation studies were conducted by Griffiths et al. (1994) on various steels under cathodic protection conditions at 22 °C (current densities about 60 $\mu A/cm^2$) to isolate such effects and to derive a critical lattice concentration for void development at which no peak was observed. Strictly speaking this is not a threshold for void development but indicates that below this concentration the rate of growth of voids is too low to register any impact on the permeation rate. With that caveat, a critical concentration for BS 4360 50D steel of between 4.0×10^{-4} ppm and 7.3×10^{-4} ppm and for AISI 4340 steel between 4.0×10^{-4} ppm and 1.3×10^{-3} ppm was deduced.

In relation to other traps for low alloy carbon steel, vacancies and solute atoms are probably of minor significance for most common steels (Grabke & Riecke 2000). Grain boundary diffusion

makes an insignificant contribution to bulk mass transport (as the effective flux is too small) and thus trapping at the grain boundary has little influence in that context. The major trap sites from a diffusion perspective are most likely associated with dislocations and with the interface between the matrix and particles (carbides, nitrides, carbonitrides) with inclusions possibly playing a role. However, the relative significance will depend on the particular composition and impurity level. Efforts to distinguish these by deforming the specimen lead to uncertainty because of opening up of interfaces as well as increasing the dislocation density. Thus, although carbides have been suggested as the primary trap sites for low alloy carbon steels (Hasegawa & Osawa 1980), the analysis of Griffiths et al. (1994) for BS 4360 50D and for AISI 4340 does not support that perception for these steels. Dislocations were considered the major trap sites in this case with binding energies between 46 kJ/mol and 50 kJ/mol inferred. Other studies (Grabke & Riecke 2000) have ascribed values of 50-60 kJ/mol to the binding energy for dislocation cores.

3.2 Estimation of C_0 values

The sub-surface *lattice* hydrogen concentration is a direct reflection of the severity of the environment and is the driving force for diffusion in the steel, which occurs by hopping between interstitial lattice sites hindered by trapping. In many studies the total hydrogen content is quoted as C_{app}, representing the sum of the trapped hydrogen (reversible) and the lattice hydrogen with the former being the dominant contribution. The derivation of total hydrogen is usually based on Fick's law but without regard to whether Fick's law applies, and thus the C_{app} value may not be at all reliable. C_{app} may reflect also the effect of trap sites that have no direct bearing on the cracking process (e.g. carbide interfaces when inclusions are the cracking sites). Since the total hydrogen content reflects trap density, binding energy and lattice hydrogen content it is not always a helpful measure, especially when comparing data for different steels exposed to different environments. This is true also for the so-called diffusible hydrogen, which reflects lattice and reversibly trapped hydrogen. The limitations become apparent when considering the total hydrogen content (C_{tot}) assuming just a dominant irreversible (denoted i) and reversible trap site (denoted r):

$$C_{tot} = C_i + C_r + C_L \tag{1}$$

$$C_{tot} = N_i \theta_i + \frac{C_L N_r}{N_L} \exp\left\{-\frac{E_b}{RT}\right\} + C_L \tag{2}$$

At steady state the concentration of irreversibly trapped hydrogen is the density of trap sites (since all trap sites then are filled by definition and the trap occupancy $\theta_i = 1$) whilst the reversibly trapped hydrogen content depends on the binding energy (E_b), density of traps, N_r, and lattice hydrogen concentration (C_L where N_L is the number of interstitial lattice sites). It is feasible for the measured trapped hydrogen (by permeation methods) not to reflect the trap sites associated directly with the cracking process though it does impact on diffusivity and thus the crack growth rate. For example, numerous studies have shown that irreversibly trapped hydrogen does not directly affect hydrogen embrittlement (Grabke & Riecke 2000, Turnbull et al. 1989). For the reasons articulated, the focus should be on determining the achievable *lattice* hydrogen content for the proposed Nagra conditions as that is the best measure of the severity of the environment and for comparison with other published work. Nevertheless, trapped hydrogen at microstructural sites or in voids will be intimately involved in the cracking process.

The time variation of the corrosion rate and its distribution over the canister surface is complex. There have been no direct measurements to determine the lattice hydrogen uptake in simulated environments and where measurements in groundwater type environments have been made these have not been at elevated temperatures. Nevertheless, the limited data are summarised in Tab. 2 (it was necessary to calculate the lattice hydrogen value from the authors' published data (Asher & Singh 2008, Cheng et al. 2000) on total hydrogen using the lattice diffusivity for pure iron). Castaneda & Leis (2007) also made measurements but did not report the membrane thickness and it is not then possible to determine the lattice concentration. Predicting the effect of temperature on these values is not readily possible as there are a number of factors involved including an effect of temperature on corrosion rate, film stability and lattice solubility. There have been numerous studies of the effect of sulphide species on hydrogen uptake in carbon steels. An example of that in the work of Cheng et al. (2000) with Na_2S (10 mg/L) is shown in Fig. 6. The solution would be just below neutral and thus addition of the sulphide should give roughly balancing concentrations of H_2S and HS^-. It is well established (Zakroczymski 1985) that sulphide species promote hydrogen uptake though in long-term experiments formation of a coherent FeS film may actually shut down the corrosion reaction and this would have contributed to the decrease in permeation current reported by Cheng et al. (2000). However, the promotion of hydrogen entry can be due also to an increased corrosion rate in addition to any effect of adsorbed sulphur species acting as a recombination poison. In the latter case the most favoured mechanism is preferential adsorption of sulphur species at surface sites such that the probability of the hydrogen atom finding an adjacent atom to recombine with is reduced, increasing the residence time at the surface and enhancing the likelihood that the adsorbed atom will "jump" into the steel.

Tab. 2: Estimated lattice hydrogen content (C_0) for different exposure conditions.

Steel	Environment	T [°C]	C_0 [ppm]	Reference	Comment
X-65 Pipeline steel (varied heat treatments)	0.5 g/L $NaHCO_3$ and 5 % CO_2 at open circuit	Room T	9.4×10^{-4} to 2.06×10^{-3}	Turnbull et al. (1989)	No indication of impact of $FeCO_3$ film
X-65	Trapped waters with 5 % or 10 % CO_2 at open circuit	25 (assumed)	1.3×10^{-4} to 2.4×10^{-4}	Asher & Singh (2008)	Other measurements suggested prior surface oxide reduced permeation current density (no data quoted) – assume steady-state, which means different solubility but not clarified Addition of Na_2S increased permeation current by factor of 2 initially and then it decreased

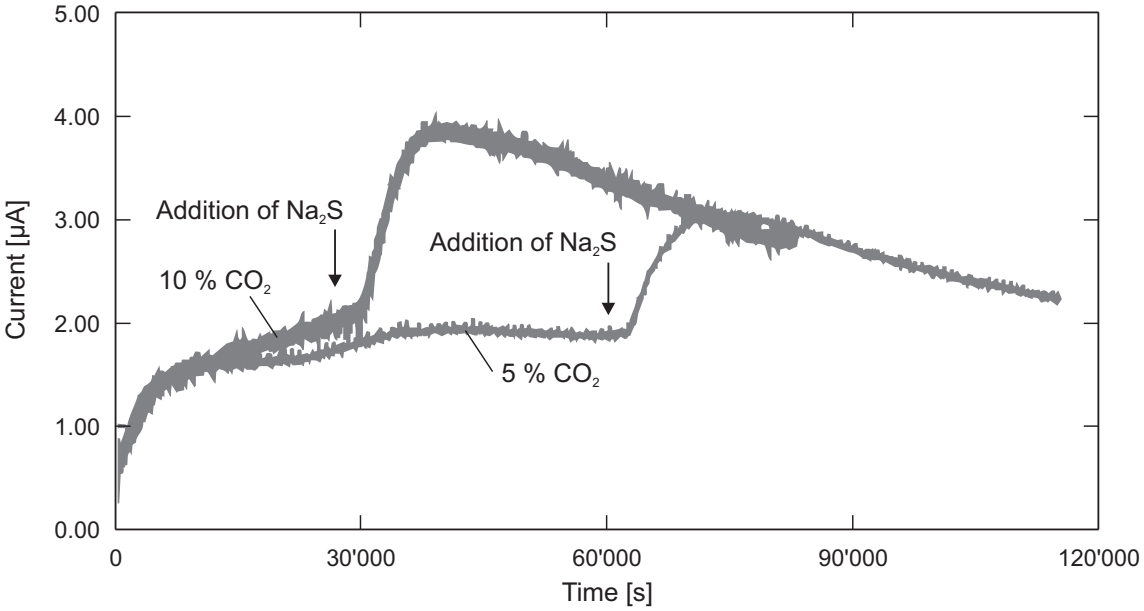

Fig. 6: Impact of sulphide addition on hydrogen permeation current for a linepipe steel exposed to trapped ground-water (Cheng et al. 2000).

The variability of the C_0 values for the two sets of data in Tab. 2 is concerning. The data of Griffiths et al. for two low alloy carbon steels cathodically protected in 3.5 % NaCl fall within that range but with current densities of about 60 µA/cm^2. Cheng et al. reported corrosion rates of about 0.18 mm/y (about 18 µA/cm^2) but the corrosion rate was not reported by Asher & Singh (2008). Clearly, prediction of the lattice hydrogen in the canister wall at temperature from hydrogen generated electrochemically is just not possible without specific measurement.

As pointed out previously, calculations have suggested that hydrogen gas pockets at the external surface of the canister may be present with pressures of about 10 MPa. In the absence of an effect of a surface film on hydrogen solubility the lattice solubility can be determined at temperature using published data for pure iron. Kiuchi & McLellan (1983) derived an expression for the hydrogen solubility in pure iron at 1 atmos. hydrogen up to 100 °C that has the form (with θ^T, the lattice solubility, in H atoms/Fe atoms):

$$\ln\left(\theta_l^T T^{7/4}\right) = -\frac{3120 \pm 90}{T} + (3.21 \pm 0.32) \qquad (3)$$

Thus, at 90 °C at 1 atmos. hydrogen gas (0.1 MPa) the concentration of hydrogen will be about 2.7×10^{-3} ppm by mass*. Assuming a square root dependence of solubility on the partial pressure of hydrogen (Sievert's law), the lattice concentration achievable at 10 MPa at the same temperature will be about 0.03 ppm. At 323 K, corresponding to 1'000 years, the value would be about 0.01 ppm and at 298 K, the calculated value would be about 6×10^{-3} ppm (higher than the values from the electrochemical permeation tests described above). In the weld metal, martensitic and bainitic regions can exist that may affect the local lattice solubility. It has not been possible to find quantitative estimates of the magnitude of the effect. Conceptually, the expected tendency is for the solubility to increase in untempered (since no post weld heat treatment) martensite as

* 1 ppm by mass is about 5.6×10^{-5} atoms H/atoms Fe.

the lattice changes from body-centred cubic through to body-centred tetragonal. Retained austenite will lead to higher local solubility in the austenite lattice but at long times the hydrogen will be in equilibrium with that in the ferrite lattice and therefore this should not impact directly on the threshold for cracking, though it does affect diffusivity. Implicitly these effects are accounted for in defining the threshold hydrogen content (in the ferrite) for cracking in welded steels.

The effect of surface films on hydrogen uptake depends on the characteristics of the film. A film may limit the available free surface, reduce the corrosion rate, impede transport of dissolved molecular hydrogen away from the reacting surface, retard hydrogen uptake due to slow diffusion though the film and reduce hydrogen solubility. If the surface film formed on the canister is porous then the primary role could be to act as a barrier to transport of reactants and products (i.e. reducing the corrosion rate) without affecting directly the intrinsic solubility, though it could reduce the effective active area. An adherent magnetite or mixed oxide film could, in principle, reduce the solubility of hydrogen atoms in the steel.

The subsurface concentration in the steel, C_0, can be defined by

$$C_0 = \frac{\theta_{ad}}{1-\theta_{ad}} \frac{k_{abs}}{k_{des}} \cdot \frac{k_m}{k_s} \qquad (4)$$

where θ_{ad} is the surface coverage of hydrogen atoms, k_m and k_s are respectively the rate constants for hydrogen transfer from the oxide to the steel and from the steel to the oxide and the absorption (k_{abs}) and desorption (k_{des}) rate constants will be for the oxide surface exposed to the environment. An $FeCO_3$ film would be expected to act as a diffusion barrier to transport of species, even in a hydrogen gas atmosphere, as catalytic decomposition of the hydrogen molecules is more likely on an oxide or steel substrate.

An important assumption in Equation (4) is that the rate of hydrogen uptake is limited by diffusion in the steel. Permeation experiments are usually designed to achieve that aim. At short times, with no hydrogen in the steel, this assumption is invalid as the flux of hydrogen is high and equilibrium sub-surface is not sustained. This is accentuated further if hydrogen charging is non-uniform as the rate of removal of hydrogen by diffusion from its source is even more effective. Hence, for the canister the kinetics of hydrogen generation may be transiently higher when corrosion is localised in the early stages of exposure but the temperature will be higher and delocalisation more effective. Thus, transiently the hydrogen concentration will be lower than predicted based on equilibrium assumptions but will approach those values at greater exposure time. Modelling, with supportive experiment, would be required to estimate the evolution of the sub-surface hydrogen content with time.

The lattice solubility of hydrogen can increase with residual stress (which is elastic), which can be significant at the weld. For iron, with a large partial molar volume for hydrogen the effect of elastic stress can be significant but for steel the effect is considered modest (Bockris & Subramanyan 1971), of order 20 %, though much greater concentration localisation can be obtained by hydrostatic stress (triaxiality, see Li et al. 1966) according to the relationship

$$C = C_0 \exp\left\{\frac{\sigma_m V_H}{RT}\right\} \qquad (5)$$

where V_H is the partial molar volume (about 2.0×10^{-6} m^3 mol^{-1}) and σ_m is the local mean stress ($\sigma_{kk}/3$). Such hydrostatic stress components may exist for defects associated with elongated inclusions. Assuming a yield stress of 300 MPa and a hydrostatic stress component ten times that (assuming crack tip stresses derived from strain gradient plasticity, see Gangloff 2003), the predicted maximum increase in C_0 would be about a factor of 8 at 90 °C. A larger factor of about 118 is predicted if locally a hard zone of yield stress about 700 MPa is assumed. However, while informative, the biggest uncertainty is in the value of σ_m, which relies on modelling assumptions that are still in a process of evolution (Gangloff 2003). Hence, while recognising that localisation of hydrogen by hydrostatic stress can occur it is not possible to put a confident estimate on it.

3.3 Diffusion and the time evolution of hydrogen in the canister wall

An estimate of the hydrogen diffusivity is required when predicting the distribution of hydrogen in the canister wall. This is essential when calculating the change in pressure of hydrogen gas in the inner chamber containing the spent fuel and the concentration of hydrogen in equilibrium with the gas phase.

3.3.1 Diffusion coefficients

Before calculating the time evolution of the internal pressure as described below, it is necessary to consider the possible magnitude of the diffusivity of hydrogen in carbon steels. In the absence of trapping the diffusivity is that for annealed pure iron. At temperatures up to about 80 °C for which the interstitial sites are tetrahedral the diffusion coefficient (cm^2/s) is given by ISO 17081 (2007)

$$D_L = 7.23\times10^{-4}\exp[-5.69\times10^{3}/RT] \quad (6)$$

In more recent work, Grabke & Riecke (2000) suggest a slightly different relationship, with an activation energy of 4.15 kJ/mol and a pre-exponential factor of 5.12×10^{-4} cm^2/s but the temperature ranged only to about 50 °C.

At more elevated temperature where the interstitial sites become preferentially octahedral, then

$$D_L = (1\text{-}2.5)\times10^{-3}\exp[-(6.7\text{-}7.12)\times10^{3}/RT] \quad (7)$$

Assuming a value of 90 °C, then the lattice diffusion coefficient based on the above equations would range from 1.1×10^{-4} cm^2/s to 2.4×10^{-4} cm^2/s.

These data provide a maximum possible diffusion coefficient.

The diffusivity in steel will depend on the number of trap sites, the binding energy (which defines the depth of the potential well relative to that of the lattice site) and the lattice hydrogen concentration (which determines the trap occupancy). As such there is no intrinsic diffusivity for hydrogen atoms in a steel (except at steady state for which diffusion is influenced only by lattice sites), as it will depend on the severity of the environment in terms of how much absorbed hydrogen it generates. For the proposed canister environment, the lattice hydrogen concentration is expected to be low and at a temperature of order of 90 °C – 100 °C reversible trap occupancy should tend to be low also. Thus, the diffusion coefficient may be described

exactly by an effective value derived from permeation experiments using Fick's law (ISO 17081 2007). At higher trap occupancy, an effective diffusion coefficient is often used but it is approximate and has no theoretical basis. This sensitivity to the environment can cause confusion when selecting data from one environmental condition and applying it to another. The activation energy also depends on trap occupancy and thence on the environmental exposure conditions. It makes comparison of datasets of hydrogen diffusivity uncertain. Added to that is concern about the reliability of some of the data as some experiments lacked rigour in eliminating uncontrolled surface effects.

Boellinghaus et al. (1995) compiled the most complete compendium of data on hydrogen diffusivity in steels as shown in Fig. 7. Previously, Coe (1973) had also compiled existing data with only small differences from that of Boellinghaus et al. (1995).

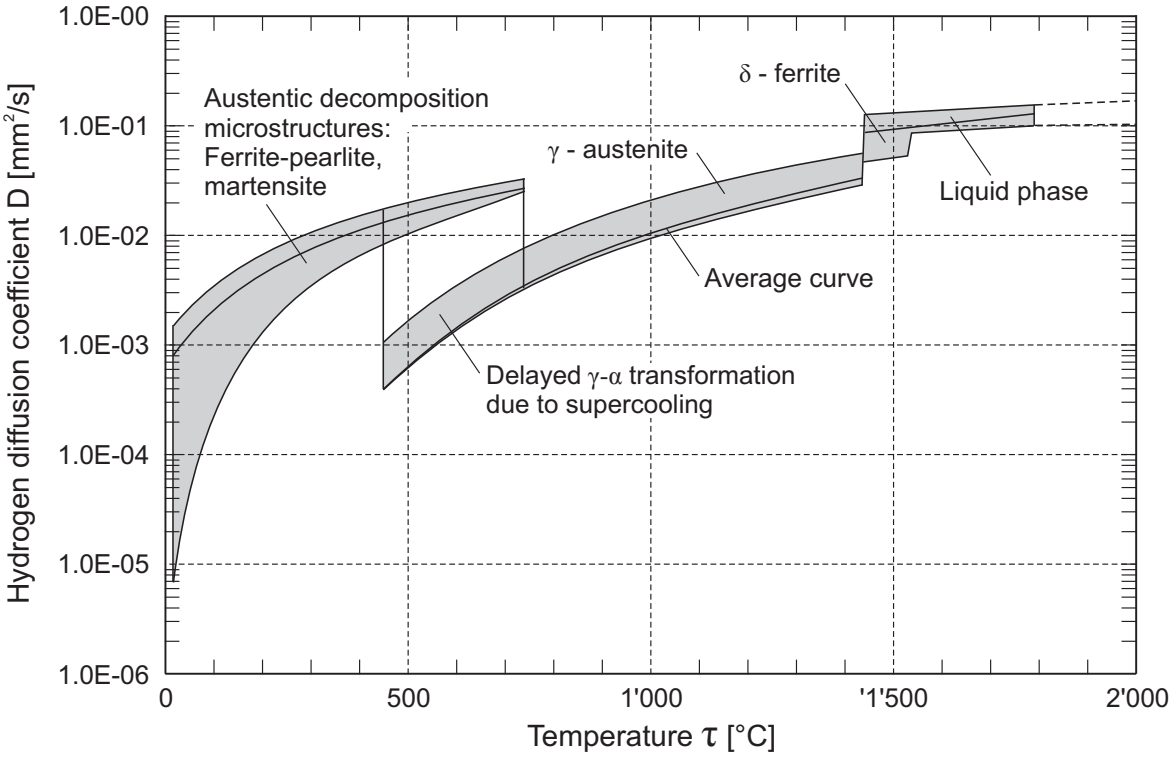

Fig. 7: Compilation of diffusion data (after Boellinghaus et al. 1995).

Because of the size of the database, filtering the data in relation to the issues above was not really feasible. For microalloyed and low carbon structural steels Boellinghaus et al. (1995) derived minimum and maximum values of effective diffusivity:

$$D_{min} = 8.8\times10^{-11}.\ \tau^{2.2285}\ \ cm^2/s \quad (8)$$

$$D_{max} = 7.6\times10^{-4}.\ \exp\text{-}(9562/RT)\ \ cm^2/s \quad (9)$$

where τ is the temperature in degrees Celsius, T is the temperature in Kelvin.

An expression for the mean value of the diffusion coefficient was obtained also but this is not much different from the maximum value and there is no special merit in adopting that relationship.

At 90 °C equations (8) and (9) would give minimum and maximum values respectively of 2.0×10^{-6} cm^2/s and 3.2×10^{-5} cm^2/s, an order of magnitude smaller than for pure iron.

At 23 °C the lower bound of 9.5×10^{-8} cm^2/s embraces measurements on X-65 steel and BS 4360 50D steel at that temperature but is not as low as that for AISI 4340 steel at low trap occupancy. The maximum value at 23 °C of 1.6×10^{-5} cm^2/s is well in excess of most published data and is likely to be applicable only for steels with very low trap density or with high trap occupancy, i.e. a very severe charging environment.

In the absence of specific data for this system at temperature, these relationships would seem a reasonable basis for first-stage calculations. They also encompass much of the variability in diffusivities measured for the HAZ. In that respect, Boellinghaus et al. (1995) point to a series of references discussing the role of microstructure on diffusivity in the HAZ suggesting for example that the high amount of carbide-ferrite interfaces in pearlite will trap hydrogen more effectively than a homogenous martensite structure but quotes other authors reporting a low diffusivity in martensite, especially for tempered martensite. Retained austenite will reduce the diffusivity also, due to trapping at the martensite-austenite interface.

The emphasis here has been on diffusion through the matrix. Although there is evidence of grain boundary transport in some very pure alloys, such as Ni, there is no compelling evidence for enhanced grain boundary diffusion in carbon steel, noting that a grain boundary in a comercial steel is also a region of significant trapping.

3.3.2 Modelling the internal pressure build-up and the hydrogen distribution in the canister wall

A rigorous evaluation of the hydrogen distribution in the steel with time is not readily possible since the boundary conditions change with time during the first 100 years or so and are not uniform over the surface during that period. Furthermore, the weld metal and HAZ will have diffusion characteristics different from the parent plate, though such local variability will have only a minor effect on the time variation of the hydrogen concentration at the internal surface. Hence, the proposed calculation of the hydrogen distribution with time should be seen as indicative.

The geometry is that of a cylinder with caps at either end. Since the diameter of the canister is very large compared with the wall thickness the conservation of species can be described using planar geometry. Assuming low trap occupancy:

$$\frac{\partial C}{\partial t} = D_{eff}\frac{\partial^2 C}{\partial x^2} \tag{10}$$

where

$$D_{eff} = \frac{D_L \exp[-E_L/RT]}{1+\frac{N_r}{N_L}\exp[-E_b/RT)]} \tag{11}$$

At the external surface the concentration is assumed to be everywhere uniform, a conservative assumption since non-uniform charging is likely. Thus,

$$t \geq 0: \; C = C_0 \tag{12}$$

The concentration at the internal surface can be described as follows:

$$t = 0: C_{int} = 0 \tag{13}$$

$$t > 0: C_{int} = kp(t)^{1/2} \tag{14}$$

where k is a constant and p is the partial pressure of hydrogen and is determined from:

$$p(t) = n(t)RT/V \tag{15}$$

where V is the volume of the gas phase in the space between the vitrified waste and the canister and n(t) is the time dependent number of moles of hydrogen gas calculated by integrating the total flux of hydrogen atoms (J) from time zero:

$$n(t) = \frac{A}{2}\int_0^t J_{int}\,dt \tag{16}$$

where A is the internal surface area.

It is envisaged that there would be a nominal 5 mm gap between the vitrified waste and the canister wall, though the design is yet to be finalised.

With R = 8.314 J K^{-1} mol^{-1} and V expressed in litres, then p is derived in kPa.

In this analysis no allowance has been made for diffusible hydrogen retained at the weld following welding as this can be configured to be relatively small and much will be lost to the external atmosphere at the elevated temperature associated with storage, even if no prior weld bake-out is applied. There may be some retention in the free volume internal region of the canister but this will be small.

A full solution of the time dependent hydrogen distribution in the steel would require numerical analysis and is beyond the scope of this review. Nevertheless, it is possible to get some estimate of the time evolution of the internal pressure using an analytical approach based on simplifying assumptions. If the build-up of internal pressure and its effect on local sub-surface concentration at the internal surface are neglected then the time to steady state diffusion in the wall can be determined for the conditions of zero concentration boundary condition at the internal surface.

An estimate of the build-up over time of the internal pressure can then be made assuming sustained constant flux at the maximum value. Normally, the steady state flux (J_{ss}) would be described by:

$$J_{ss} = \frac{D_L C_0}{L} \tag{17}$$

where L is the wall thickness. However, given the nature of the approximation it would be more appropriate to use the effective diffusivity rather than the lattice value as it is more likely to reflect better the true time evolution. It would be more satisfying to solve the problem rigorously as one limiting approximation then sets a requirement for another.

Nevertheless, the assumed boundary condition of zero concentration at the inner surface gives a maximum flux of hydrogen and allows determination of an upper bound value for the rate of pressure increase. That at least would indicate whether a more rigorous analysis was justified.

The time-dependent pressure of hydrogen molecules inside the canister, *P(t)*, is given by:

$$P(t) = J_{ss} \frac{A}{2} \frac{RT}{V} t \qquad (18)$$

Values calculated using this approach are given in Tab. 3, for which a free internal volume of about 55 L (0.055 m^3) is assumed corresponding to a 3.25 m long canister. It should be noted that the time to achieve a linear profile through the wall based on $D_{eff} = 2\times10^{-6}$ cm^2 s^{-1} was less than 1'000 days, and thus, for this limited analysis Equation (17) with D_{eff} could be used for long times without significant error in that context.

Tab. 3: Approximate estimates of time evolution of pressure in a HLW canister of length 3.25 m at 90 °C, assuming zero concentration boundary condition at inner surface and a value of 0.03 ppm (2.37×10^{-7} moles/cm^3) at the outer surface, L = 15 cm, internal radius = 35 cm and internal length = 295 cm..

D_{eff} [cm^2 s^{-1}]	**Time** [y]	**P** [MPa]
2×10^{-6}	100	0.13
	1'000	1.3
	7’462	10
3.2×10^{-5}	100	2.2
	467	10

It is evident that attainment of a pressure within the canister equivalent to the external pressure is feasible within 1'000 years assuming the upper bound flux and diffusion coefficient. While a more reliable estimate can be made based on a rigorous analysis, and that will predict a longer time, possibly about a factor of 2 higher, it is still likely that high internal pressure will build up in the relevant timeframe if the diffusivity is high. Thus, the local sub-surface concentration of hydrogen atoms at the root of any weld should be considered to be similar to that at the external surface at long times but at short times the inner free volume acts as a sink for hydrogen atoms thereby decreasing the local dissolved concentration at the inner surface of the weld.

These estimates have to be qualified in view of the progressive decrease in temperature to about 50 °C over the 1'000-year period. However, given the large spread in diffusivities it is not of value to be too refined in the calculations at this stage but to recognise that diffusion is potentially fast enough to achieve equilibrium pressures in the inner chamber and that it would be prudent for the purposes of the evaluation of cracking propensity to adopt that perspective.

No consideration has been given here to the effect of oxide films on hydrogen diffusivity. In view of the small thickness of the oxide relative to the wall thickness of the canister any effect of a reduced diffusivity in the oxide on the rate of permeation will be confined to a short exposure period when the flux in the metal is high for which surface effects become more rate limiting. It becomes of no significance at longer times. This underpins standard permeation tests for which the requirement is that the membrane be thick enough to eliminate any effect of oxide transport (ISO 17081 2007). It is not possible to calculate the magnitude of the effect since specific data are not available but it makes sense to ignore any benefit as it cannot be assured.

3.4 Summary of Section 3

- At short times where localised corrosion can be envisaged and the corrosion rate may be transiently high, relative to long term exposure, the hydrogen generation rate could be correspondingly high. However, due to the high diffusivity at the exposure temperature and delocalisation of hydrogen from a non-uniform source this does not mean necessarily that the local sub-surface hydrogen content will be large. Predicting the value is non-trivial.
- At longer times, a value for the dissolved hydrogen atom concentration in the steel of about 0.03 ppm at 90 °C would seem a reasonable estimate based on gas solubility and a gas pressure of 10 MPa. There are no data at this temperature that allow determination of the dissolved hydrogen generated electrochemically but there is no basis for thinking it would be larger than for the gas. Intriguingly, if smaller this would create internal hydrogen concentration gradients in the steel that would ultimately affect the electrochemistry. At 1'000 years, the temperature will have decreased to about 50 °C at which the lattice solubility will have decreased to about 0.01 ppm.
- Trap occupancy will tend to increase with the decrease in temperature and is often a reason for the greater propensity for hydrogen assisted cracking at low temperatures (in terms of threshold – see Section 5.1). Thus, it might be anticipated that cracking susceptibility may be greatest at long exposure times for the waste canisters. However, the actual trap occupancy dependence on temperature will be a function of C_0, which decreases with decrease in temperature, and the magnitude of the binding energy for the critical trap site (unknown for this system). Hence, *a priori* assumptions cannot be made but it seems likely that the greatest sensitivity to cracking may be at long times because hydrogen uptake will be more uniform and trap occupancy will probably be greater.
- Sulphur species are known to impact on corrosion rate and on hydrogen uptake. For the steel canister the impact of sulphur species on overall corrosion losses is expected to be very small. However, it is more difficult to conclude definitively that at all exposure times, especially the early stages, the impact on hydrogen uptake is wholly insignificant.
- At 90 °C, values for the effective hydrogen atom diffusion coefficient in carbon steels would range from 2.0×10^{-6} cm^2/s to 3.2×10^{-5} cm^2/s, the range reflecting different trapping characteristics of the steels and possibly just variability in the quality of the data.
- On the basis of the maximum value for D_{eff}, attainment of internal pressures in the inner chamber matching that externally is feasible within 1'000 years. Whilst a decrease in temperature will occur over this period there is sufficient uncertainty in the diffusivity data that it would be prudent for the purposes of this analysis to assume diffusion will be potentially fast enough to achieve equilibrium pressures.

4 Review of hydrogen related degradation mechanisms for C-steel

Cracking occurs when critical combinations of local hydrogen content, stress, strain, and microstructural sensitivity are achieved. The precise mechanism depends on the particular system and includes development of pressure of hydrogen gas at internal voids (hydrogen-induced cracking, HIC, or stress oriented hydrogen-induced cracking, SOHIC), hydrogen enhanced decohesion (HEDE) of Fe-Fe bonds, hydrogen-affected localised plasticity, as introduced initially by Beachem (1972; adsorption induced dislocation emission, AIDE, or hydrogen enhanced localised plasticity, HELP). These mechanisms are not mutually exclusive in some cases. Hydride formation (Birnbaum 1990) can arise in some alloys (Group 4 and Group 5 metals of the Periodic Table) such as titanium, but is not relevant to carbon steels.

The value of understanding the mechanism is that it might allow metallurgical modification of the microstructure to induce improved resistance, provide a basis for quantitative prediction, and enable a framework for rationalising the fractography of failure, where this is relevant.

4.1 Hydrogen-induced cracking (HIC) and stress oriented hydrogen - induced cracking (SOHIC)

The underlying concept of the internal pressure mechanism is that hydrogen atoms recombine to form molecular hydrogen at internal voids or fissures. These voids may be pre-existing cavities formed at interfaces during processing. However, it is possible in the presence of stress to envisage a mechanism of micro-void development arising from a combination of strain localisation at inclusions, particles or at Fe_3C/ferrite phase boundaries, and trapped hydrogen at the interface. The concentration of the latter may be further enhanced if there is a significant hydrostatic stress component at some location around the interface. If there is sufficient fugacity of the dissolved hydrogen in the void then the pressure attained can be large enough in the void to develop a crack. These cracks tend to form in-plane in the forged or rolling plane, often in colonies, and given the orientation may not intrinsically be damaging in some cases. However, failure occurs because these crack colonies interlink to form an extended through-thickness crack.

In the absence of significant stress (HIC) these cracks interlink through shearing at 45° to the crack tip to give a stepwise appearance (Dewsnap et al. 1987); thus, the terminology step-wise cracking. However, if there is residual or applied stress present, that stress may not only enhance localisation of hydrogen but may change the manner in which the individual cracks link up (Iino 1978). In this case (SOHIC, see Iino 1978 and Cristensen 1999), the linked cracks tend to form a stack (almost ladder–like) because the location of maximum shear stress moves away from the tip of the small crack to mid-way along the crack (Pargeter 2007). A schematic of the crack morphology is reproduced in Fig. 8, with the emphasis on H_2S applications Oriani (1990).

The process of crack linking could be enhanced by an AIDE or HELP mechanism. It is evident that HIC is a precursor to SOHIC but Pargeter (2007) notes that SOHIC can occur in materials resistant to HIC because stress can open up interfaces, e.g. in pearlite colonies, that might otherwise be intact. This presumably occurs by strain localisation, e.g. by a HELP mechanism, and most commonly in the softer region of weld HAZs. Pargeter (2007) states that through-thickness stresses are able to form in locally softened material through strain concentration. However, this statement is not transparent; strain localisation can occur in softer regions in response to external stresses in a material with differential hardness but it is less obvious that

this strain localisation can be induced by residual stress. The presence of stress will also reduce the hydrogen fugacity required to propagate a crack, though in the literature on both HIC and SOHIC it is surprising that less emphasis is given to the impact of the local dynamic plastic strain implicit in the void growth process.

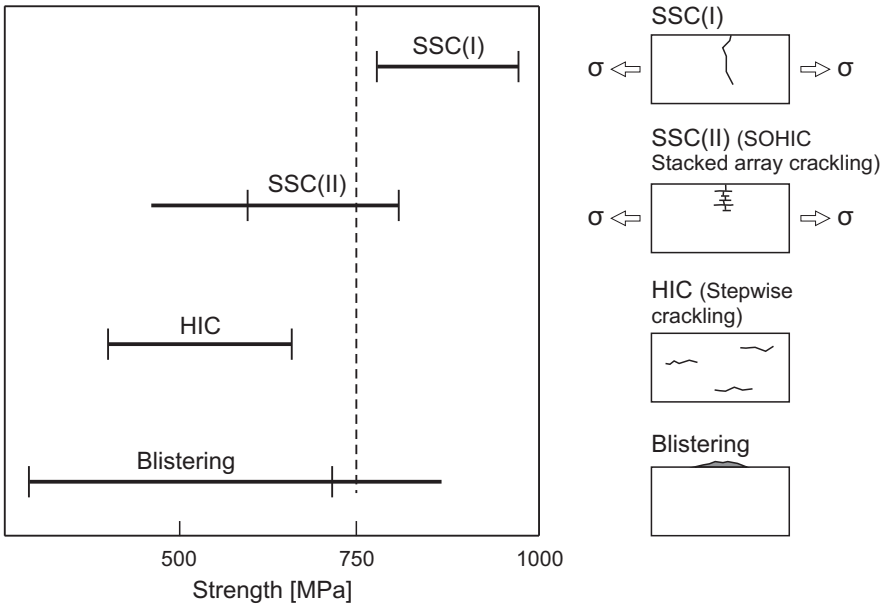

Fig. 8: Schematic of sulphide stress cracking (SSC), SOHIC and HIC processes (after Christensen 1999). Type I is considered to represent failure in high strength steels and Type II to represent failure in medium and low strength steels in what was later termed SOHIC. Blistering is associated only with very severe charging in acidic H_2S environments and is not applicable to this waste containment application.

The rate of propagation of both HIC and SOHIC will depend on the rate of supply of hydrogen to the voids/cracks. This will be determined by the trapping characteristics of the steel, which will include also the density and volume of the voids/cracks, and, thus, will be time-dependent. No reliable models exist to quantitatively predict the rate of crack advance but considerable insight into the role of microstructure enables qualitative prediction of which microstructural features are liable to lead to cracking.

HIC and SOHIC are usually considered as mechanisms appropriate to low to medium strength carbon steels and their welds. This follows because of the increased hydrogen pressure required for the development of voids in a high strength steel, where yielding is more restrained. Nevertheless, HIC can occur for steels of relatively high strength (Fig. 8) if the hydrogen uptake is large and/or the microstructure/microchemistry particularly poor. Thus, Dewsnap et al (1987) highlighted a number of examples of HIC at strength levels up to 784 MPa and drew the conclusion that failure can occur even at the higher strength level with the inappropriate combination of inclusion density, morphology and other microstructural features. Hard zones in welds will mean locally higher strength levels and sharper defects/voids with higher stresses, which means that the hydrostatic stress component that localises hydrogen to the tip will be greater.

4.2 Hydrogen enhanced decohesion (HEDE)

The concept of hydrogen enhanced decohesion (Oriani 1990 and Gangloff 2008a) is that dissolved hydrogen atoms accumulated in the hydrostatic stress zone at the crack tip achieve such high concentrations that they lower significantly the cohesive binding force between metal atoms. Cleavage of these bonds occurs when the local tensile stress just ahead of the crack tip is greater than the reduced cohesive force resulting in tensile separation of atoms rather than slip. Impurities may also play a role in some systems; for example S at grain boundaries can reduce the interatomic bond strength and can add to the embrittling effect of hydrogen. Initially it was considered that it was simply lattice hydrogen that was critical, driven to the crack tip region by very high hydrostatic stresses, but this has moved on to a recognition that hydrogen trapped at microstructural sites in the "fracture process zone" would more likely provide the required hydrogen concentration, allied with the higher lattice concentration (Turnbull 1993). These sites have to be specific since irreversible trap sites can generate high local concentrations but do not feature directly in the cracking mechanism. Indeed, the finer details of the mechanistic process are not as well expounded as would be desirable and predictive models to describe K_{th} (threshold stress intensity factor) and da/dt (crack growth rate) involve adjustable parameters (Gangloff 2008a and Turnbull 1993). It is also very difficult to design an experiment that can offer proof that cleavage (bond-breaking) due to hydrogen does actually occur. As a consequence, evidence in support of the concept is often indirect. Nevertheless, phenomenologically, a combination of sharp crack tip, high concentration of hydrogen atoms and very high stress is required. For this reason, this mechanism is a likely candidate only for high strength alloys, and not for the low strength carbon steel appropriate to the canister.

4.3 Adsorption induced dislocation emission (AIDE)

Lynch (2007) proposes that crack growth occurs by the adsorption induced dislocation emission (AIDE) mechanism. He considers that "adsorbed" hydrogen atoms (adsorbed here means strongly-bound hydrogen in the first few atomic layers) weaken substrate interatomic bonds (note parallel with decohesion concept but with different consequences and lower required stresses) and thereby facilitate the emission of dislocations from crack tips. This gives rise to small voids at particles or at slip-band intersections. The crack path could be transgranular or intergranular depending on where dislocation emission and void formation occur most readily. For transgranular cracking, crack growth occurs primarily by alternate slip from crack tips (to minimise the back stresses from previously emitted dislocations) with contributions from general plasticity and void formation ahead of cracks. The mechanism is also considered to be feasible from internal voids containing hydrogen. Supportive arguments for this mechanism have been based mainly on interpretation of fractography and of similarities between liquid metal embrittlement and hydrogen assisted cracking in some systems. However, the relevance of this mechanism is significantly debated (Gangloff 2003). As with HEDE, there is no direct evidence for an effect of adsorption on dislocation emission. The primary limitation of the model is the lack of a quantitative framework for threshold or crack growth rates. In relation to the implications of the mechanism for the effect of microstructure, Lynch (private communication S.P. Lynch, 2008) suggests that limiting the number of possible sites for void development, i.e. clean steels, would be pertinent and in relation to crack growth benign traps that constrain diffusivity would of course be beneficial, though that is apparent for any mechanism. Reducing the strength level to encourage crack-tip blunting processes would also be inferred.

4.4 Hydrogen-enhanced local plasticity (HELP)

The concept of hydrogen-enhanced local plasticity (Birnbaum 1990, Ferreira et al. 1998 and Robertson 2008) envisages dissolved hydrogen enhancing the *mobility* of dislocations resulting in highly localised deformation. Failure is considered to occur by a shear process but, due to the localisation, the fracture surface appears macroscopically brittle. Gangloff (2003) highlights the difference between HELP and AIDE in that for the former dislocation *mobility* is enhanced around dislocation cores resulting in reduced elastic energies of interaction between moving dislocations and a variety of obstacles. For the AIDE, it is a dislocation *nucleation* process. Robertson (2008) presented convincing evidence for the basic physics of the process, showing that even with pre-deformed alloys, with high dislocation density at cell walls, addition of hydrogen gas could lead to ejection of dislocations. Furthermore, dislocations at grain boundaries were shown to move under the influence of hydrogen. In all cases, they argue hydrogen enhances the movement of dislocations (not their nucleation) and increasing the hydrogen pressure induces an increase in dislocation velocity. Cross-slip is also enhanced. An interesting experiment was to show that S at the grain boundary of nickel could in combination with hydrogen reduce slip across the interface leading to strain localisation and embrittlement. There have been convincing experiments that demonstrate the basic premise. However, in some cracking experiments with hydrogen pre-charged specimens tested in air (Murakami 2008 and San Marchi et al. 2008) the perceived observation of a HELP mechanism has to be qualified by the nature of the tests. In these tests, the concentration of hydrogen right at the crack tip may be relatively low as it escapes to the outside atmosphere, thus favouring an internal cracking mechanism as distinct from a near-surface process that might prevail when the source of hydrogen is external. Nevertheless, the evidence for the basic process is quite convincing. What is lacking is a demonstration that that is the controlling factor (as far as crack growth is concerned) in a particular system. Also, there is no predictive feature of this model in relation to da/dt or threshold (though void growth models are being developed, see Liang et al. 2004) and that could be considered implicitly to apply to the impact of other metallurgical variables such as strength level and microstructure.

4.5 Summary of Section 4

- HEDE is not envisaged as a mechanism for cracking of low strength carbon steels and by implication, their welds also.
- HIC would be the most likely mechanism for cracking in a low strength carbon steel in the absence of applied dynamic strain but only if there is sufficient hydrogen introduced into the steel (see Section 5.2.1) and if there is a hydrostatic stress component able to accumulate the required concentration of hydrogen to cause sustained void development. The growth of the void will create a local dynamic plastic strain and that could influence crack growth.
- Linkage to form through-thickness cracks occurs by a slip process that could be induced/enhanced by AIDE or HELP. The linkage of the voids will depend on stress and SOHIC is feasible.
- Extensive information exists on the impact of microstructure on HIC but this is less well developed for other mechanisms.
- None of the mechanisms offers a robust basis for quantitative prediction of threshold or crack growth rates and such predictive models that do exist have not been used in an engineering context.

5 Threshold conditions for cracking

The threshold conditions for cracking will involve a combination of applied and residual stress, stress concentration, hydrogen uptake and material characteristics, including the HAZ and weld metal.

Domain diagrams to relate the cracking susceptibility of carbon steels to the combined influence of hydrogen uptake and yield strength have been generated (JNC 2000) as exemplified by Fig. 9. There is an attractiveness in such a simplified approach but the hydrogen concentration should be the lattice value (not the total hydrogen as was adopted in producing this figure) and the effects of welding, localised corrosion, temperature, steel composition and concentration of impurities need to be accounted for in defining the boundaries. This combination of factors suggests constraint in the direct application of this specific diagram to the assessment of cracking likelihood for the waste container steel. A step-by-step approach to determining the threshold conditions for cracking that accounts for the variables will provide more confidence in prediction.

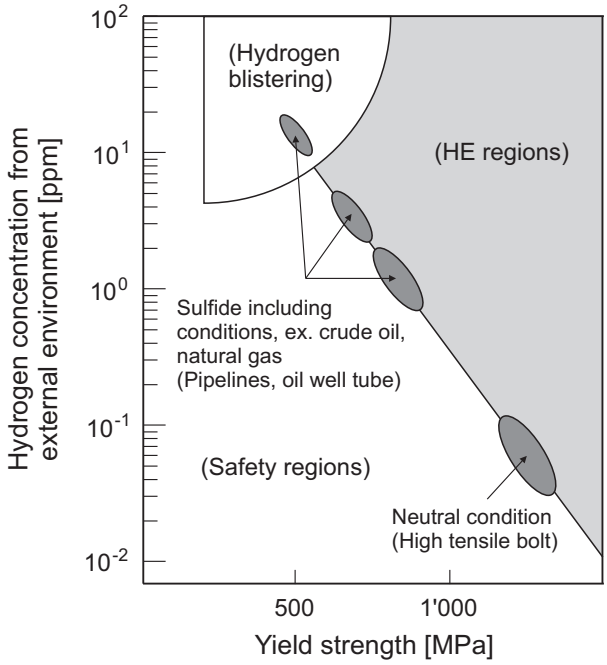

Fig. 9: Schematic illustration of the zones of susceptibility of carbon steel to hydrogen related degradation mechanisms (JNC 2000).

The design stress for this system (Johnson & King 2003) is of the order of 30 MPa and this would be considered relatively insignificant as a primary driving force for hydrogen assisted cracking. The major stress will be the residual stress following welding. Intrinsically that stress is elastic and will not exceed the yield stress of the steel, once cooled. Hence, based on present ideas about the selection of the steel, one might estimate a maximum residual stress of about 235 MPa. However, this does not account for hardening associated with the HAZ and it is feasible to generate residual tensile stresses that approach yield for the locally hardened material associated with bainitic or martensitic microstructures. Hardness depends primarily on the hardenability of the steel (determined by its composition) and the cooling rate, so it can be managed to an extent by alloy selection and optimum welding practice.

The issue then is the extent to which the residual stress can assist the initiation and propagation of cracks from pre-existing weld defects, surface defects or corrosion pits (recognising that initiation of hydrogen assisted cracking from a relatively smooth surface, with no hydrostatic stress component can be difficult, see Magnin & Najjar 1995) or from voids generated via a HIC type mechanism. Treating HIC as separate for the moment because of the dynamic and self-stressing characteristic nature of the defects, the threshold stress for cracking is best described by the following schematic diagram (Fig. 10; Kocak et al. 2008).

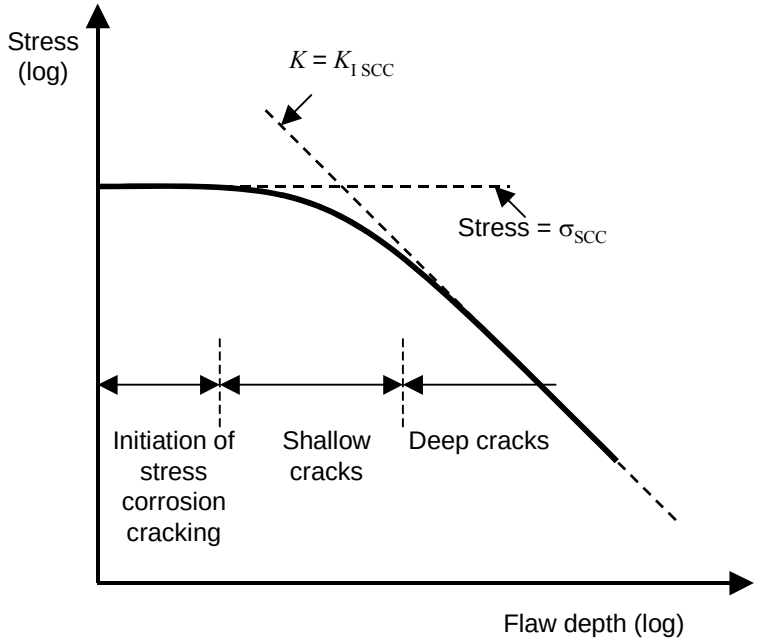

Fig. 10: Modified Kitigawa-Takahashi plot showing the threshold stress for stress corrosion cracking as a function of crack size.

A crack will continue to propagate if the stress-crack size combination is above the full line (Kocak et al. 2008).

Here, σ_{SCC} is the threshold stress above which any initiated crack will continue to propagate and K_{ISCC} is the threshold stress intensity factor for sustained crack growth (above this value any initiated crack will continue to grow and below, growing cracks will arrest). Most threshold data for hydrogen assisted cracking are based on K_{ISCC}.

5.1 Threshold stress intensity factor

The lower bound threshold stress intensity factor for various steels in different charging environments as a function of yield strength is shown in Fig. 11. Data from 400 measurements for a range of steels and environments have been captured in this plot (Gangloff 2003). The data for high pressure hydrogen include fugacities as high as 180 MPa and these are setting the threshold values in that case.

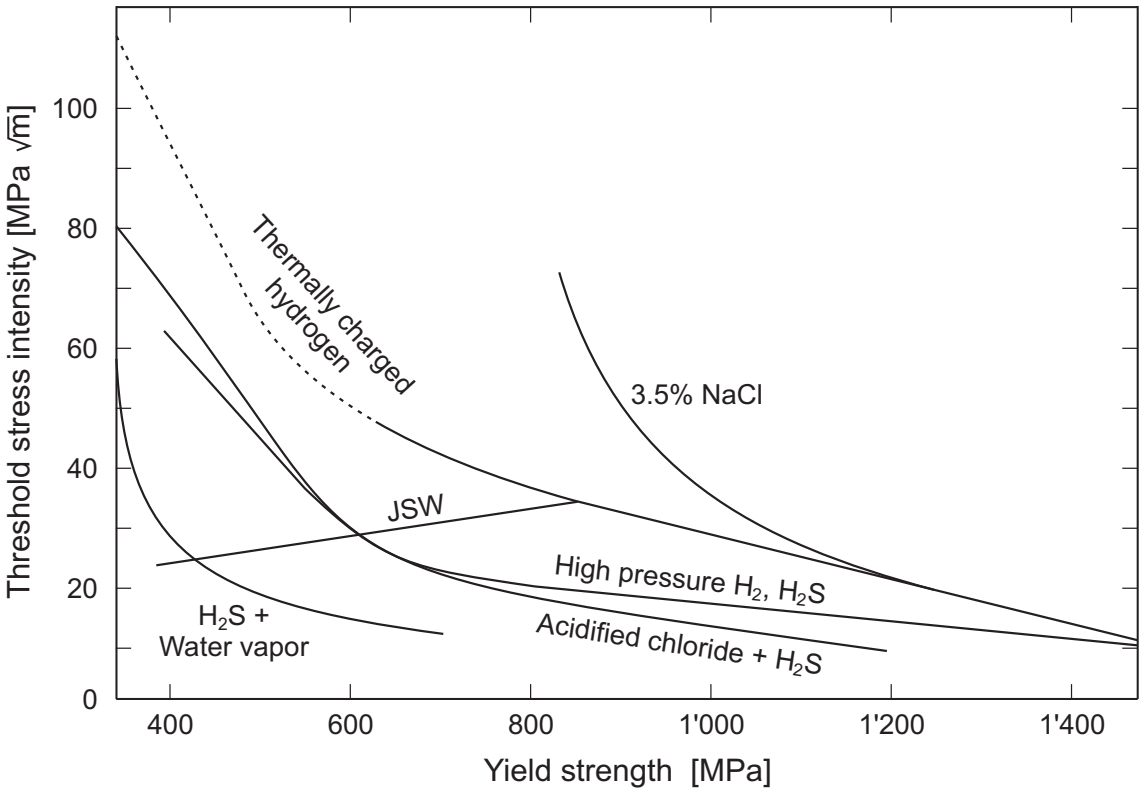

Fig. 11: Lower-bound trends drawn to represent the results of over 400 measurements of the threshold stress intensity factor for internal and external hydrogen assisted cracking at 23 °C (after Gangloff 2003). (JSW – Japan Steel Works)

The JSW line refers to measurements from the Japan Steel Works under rising crack mouth opening displacement (CMOD) test conditions but the trend is supported by similar results from Gangloff (2008b). For the rising CMOD tests, the crack tip is being dynamically strained and this is often a more severe test, especially for the lower strength steel that otherwise would not crack under static load. There are two factors here, the rate of generation of new oxide-free surface promoting increased hydrogen entry and possible dislocation transport of hydrogen in the process zone at the crack tip.

An example of the data-set most relevant to the 10 MPa pressure expected for the canister are the K_{th} values as a function of pressure of hydrogen gas (expressed as a fugacity) at different strength levels as shown in Tab. 4 (Gangloff 1986). The strength levels span values close to the parent steel for the canister and possible values in a hardened zone in the HAZ. There is no particular explanation for the higher value at 634 MPa relative to that at 669 MPa.

These data were derived at 23 °C or thereabouts. With increasing temperature, the threshold stress intensity factor for cracking in hydrogen gas tends to increase. An example (San Marchi & Somerday 2008), albeit for a high strength steel, is shown in Fig. 12. The temperature dependence of cracking is complex. With increasing temperature the hydrogen lattice solubility increases (in aqueous environments the corrosion rate may also increase though this may be affected by film stability) but the trap occupancy decreases. The ductility will also increase with temperature. In terms of hydrogen concentration in the steel, the lower content of the traps is probably the dominant factor and the primary explanation for the increase in threshold stress intensity factor with temperature in hydrogen gas. The crack growth rate variation with

temperature is more complex, increasing initially from ambient temperature but then exhibiting a maximum (Gerberich et al. 1988). Here, it is the rate-limiting factor that is important. Thus, in addition to trap concentration the rate of diffusion is important and that increases significantly with temperature, because of reduced trap occupancy to a large extent.

Tab. 4: K_{th} for different strength steels as function of hydrogen fugacity at room temperature (San Marchi et al. 2008).

Strength level [MPa]	**Pressure** [MPa]	**Fugacity** [MPa]	**K_{th}** [MPa $m^{1/2}$]
300	3.5	3.6	131
	6.9	7.6	111
	20.7	23.5	98
634	21	23.9	87
669	21	23.9	71
724	21	23.9	96

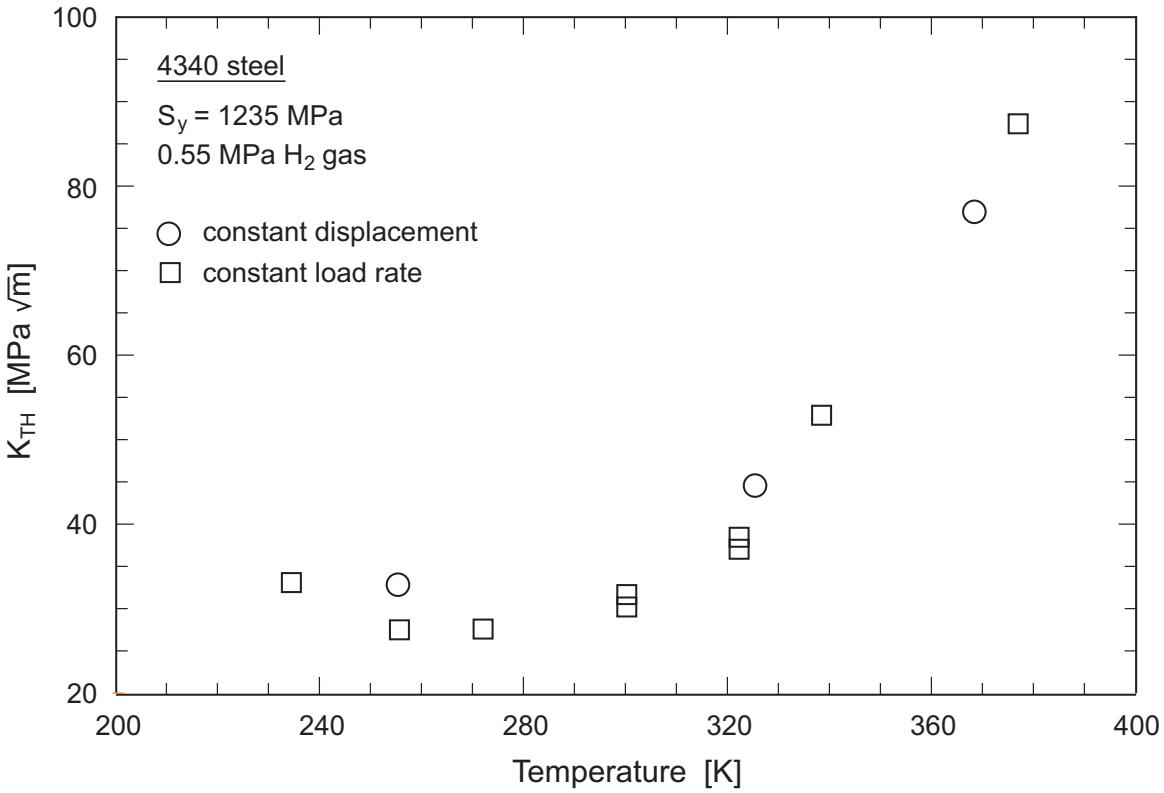

Fig. 12: Temperature dependence of K_{th} for 4340 steel in hydrogen gas (after San Marchi & Somerday 2008).

Now consider the possible value of the stress intensity factor that might be envisaged. Pre-existing surface defects of depth greater than 2 mm would be very unlikely to be missed by non-destructive evaluation (NDE). Although defects of this size should not be introduced in carefully welded components it makes sense to adopt such a value for integrity analysis. It will be assumed that the local yield stress of hardened steel in the HAZ will not exceed 700 MPa, as a worst case, including any effect of surface grinding of the weld cap, which is controllable and should be optimised to minimise surface-hardened regions of high residual stress. This figure of 700 MPa will be the maximum value for the residual stress. On that basis, and assuming the simple relationship of $K = \sigma\sqrt{(\pi a)}$, the expected K value would be about 55 MPa $m^{1/2}$. This is significantly lower than the threshold values in Tab. 4, noting also that the data in the table relate to room temperature values.

The data for pitting can also be used, though recognising that pitting as a source of possible cracking has to be located at the weld, where significant residual stress might arise. Quoting the JNC report, Johnson & King (2008) suggest that maximum pit depths in the range of 1 cm might be attainable in 1'000 years. Using analysis for the approximate value of K for a pit ($K = \alpha\sigma\sqrt{(\pi a)}$, see Toyama & Konda 1989 and Kawai & Kasai 1995), this would infer a K value of 83 MPa $m^{1/2}$ with α, a geometric factor, taken to be 0.67 corresponding to a hemispherical pit This is a relatively high value compared with the threshold K indicated in Tab. 4. However, it assumes that the deepest pit coincides with the region of significant residual stress and ignores the relaxation of that stress by the growing pit (this beneficial relaxation should be discounted as this would apply also to cracks but residual stress does lead to failure). Also, the transition from a pit to a crack is a complex process (Kondo 1989) and not represented simply by a threshold pit depth and K value. Furthermore, Johnson & King (2008) argue that deep pits in the conventional sense are unlikely and the perception should be of pits of a small aspect ratio (depth to opening) more akin to surface roughening. This can be encapsulated in the pitting factor (ratio of maximum depth of corrosion to the average depth of corrosion), which is shown to decrease with decreasing depth of corrosion (i.e. the corrosion becomes more uniform), Fig. 13. This would suggest that stress concentration should be modest. The temperature is also elevated (about 50 °C after 1'000 years) and so the K_{th} would be somewhat higher than in Tab. 4.

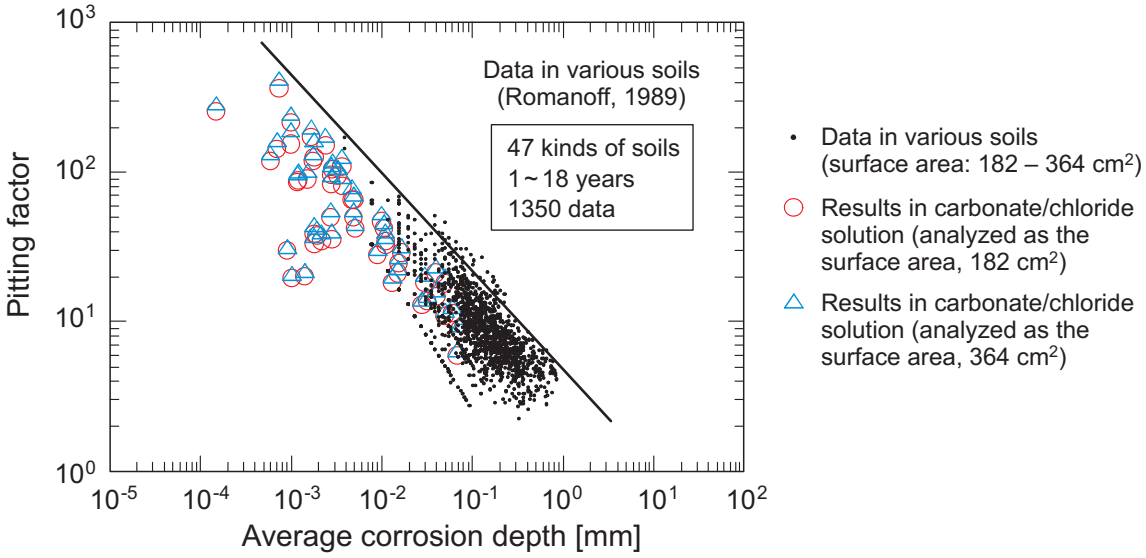

Fig. 13: Variation of the pitting factor with the average depth of corrosion derived form long-term corrosion tests and short-term laboratory measurements (from Johnson & King 2008, based on JNC 2000).

Nevertheless, given the uncertainties in the extent of uniformity of corrosion and the complex early exposure history of the canisters it may be prudent to assess the implications of the worst-case scenario since it may be argued that pits are not smooth (except under high current density polishing conditions) and local regions can dissolve preferentially (and transiently) within a pit if the microchemistry is favourable. Conceivably this could lead to stress and strain concentration within the pit. Clearly, mitigating the possibility of hardened zones in welding and high residual stresses should be an objective.

The analysis above focuses on very deep pits and high stresses. In a stress field, a growing pit may induce a dynamic plastic strain with a strain rate dependent on the pit growth rate such that the threshold for cracking is reduced. However, where the stress field is predominantly residual such a dynamic plastic strain could not be sustained as by implication relaxation of residual stress would be occurring. Nevertheless, it is a wholly unexplored concept and creates an uncertainty, though it would require a combination of adequate pit depth, growth rate and residual stress level to be effective.

5.2 Threshold conditions for hydrogen-induced cracking (HIC) and stress-oriented hydrogen-induced cracking (SOHIC)

On the basis of Fig. 11, it might be deduced that crack propagation in the absence of externally applied dynamic strain (see also Hinton & Proctor 1983) would not be possible in low strength steels yet HIC and SOHIC do occur.

HIC and SOHIC are observed commonly when high hydrogen fugacities are obtained in the steel, usually in H_2S-containing acid solutions, though it will be noted that Fig. 11 does also refer to such solutions. A possible reconciliation of the data in Fig. 11 with HIC observations for low strength steels is that void expansion associated with increasing hydrogen gas pressure creates a dynamic plastic strain locally, which then lowers the local threshold stress intensity factor for cracking, in a manner reflected in the rising CMOD data. For internal voids, oxide rupture is not a factor.

Since the threshold *mechanical* driving force for HIC is intrinsically related to the environmental conditions and the detailed characteristics of the microstructure, especially particle/ inclusion shape, the local value will be unknown and it is more pertinent to think in terms of a threshold hydrogen uptake relative to a particular microstructure (and hardness) as a criterion for assessing the risk of cracking.

In that context the literature up to 1987 on HIC for pipeline steels was reviewed comprehensively by Dewsnap et al. (1987) and a recent more succinct review by Herrmann et al. (2005) has since provided a useful update. The key features from these are now summarised.

5.2.1 Threshold hydrogen concentration for hydrogen-induced cracking

The review by Herrmann et al. (2005) is useful in defining a threshold hydrogen content for HIC.

Hermann et al. reported data for the critical "hydrogen permeation coefficient" as a function of hardness in a simulated segregation zone for a pipeline. The permeation coefficient used here is $i_pL = FD_LC_0$ with units of A/cm where i_p is the steady-state permeation current density, L is the thickness, F is Faraday's constant, D_L is the lattice diffusion coefficient and C_0 is the lattice concentration of hydrogen subsurface. To convert the data of Hermann et al. as expressed in

Fig. 14(a) and 14(b), note that 10 μA/cm for a 0.6 cm thick membrane is equivalent to a lattice C_0 value of 1.8 ppm. In NACE Solution A (NACE TM0284), a value of 15-18 μA/cm was measured. Using this relatively severe environment a threshold hardness of 320-350 HV was identified.

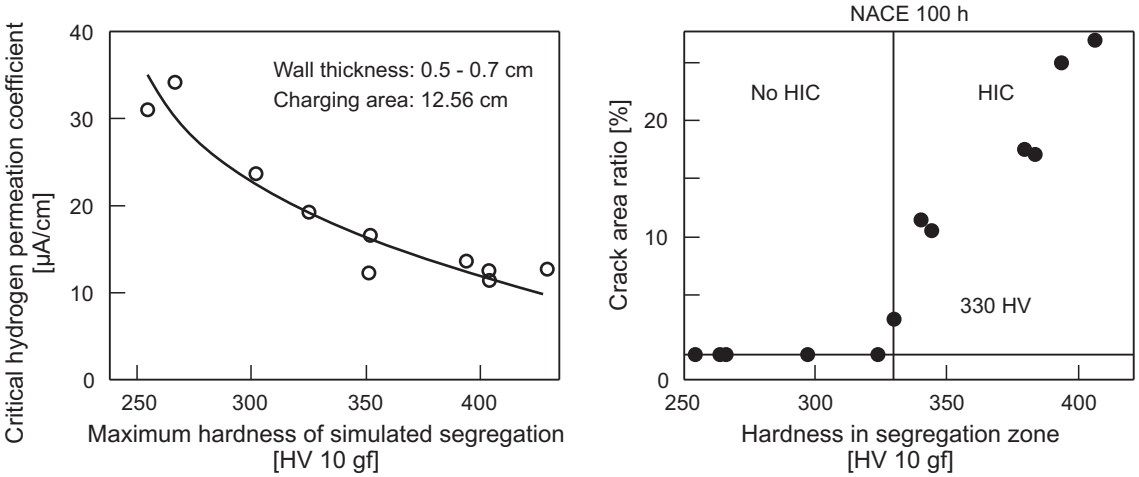

Fig. 14: Critical hydrogen permeation coefficient (a) and Crack Area ratio (b) as a function of hardness in simulated segregation zone (after Takeuchi et al. 2004 *cited in Herrmann et al. 2005*).

When comparing the figure of 1.8 ppm lattice hydrogen with the estimated lattice concentration for the waste containment steel of about 0.03 ppm (albeit based on equilibrium with hydrogen gas pockets) this would be very reassuring. However, it can be misleading to generalise these data because the results were based on a modern steel designed for linepipe applications and cannot be applied to steels in general simply because of the range of possible compositions and MnS contents. For example, the results of Elboujdaini et al. (2003) indicate threshold concentrations as low as 0.27 ppm in a steel with a high inclusion content. It may be inferred from the paper that this is the total hydrogen concentration; there was not enough information to convert this to lattice hydrogen content.

Defining a lower bound lattice hydrogen content that would cover a range of meaningful composition and impurity levels for comparison with that projected for the waste canisters is not possible. Although there are sets of data on HIC where hydrogen uptake has been measured, too much of the available data is based on total hydrogen and does not allow extended prediction.

5.2.2 Threshold hydrogen concentration for stress oriented hydrogen-induced cracking

While there are data for the threshold hydrogen content for HIC, such information does not exist for SOHIC because of the sensitivity to applied and residual stress as well as the material characteristics. Nevertheless, it is often stated (Cristensen 1999 and Pargeter 2007) that severe charging environments are required; for example, acid solution with H_2S.

5.2.3 Threshold temperature for hydrogen-induced cracking

HIC is considered to be a phenomenon that prevails most significantly at about 20 °C or so and is often considered to be negligible at 60 °C based on laboratory studies as cited in Li et al. (1966). These latter laboratory and service results would tend to be in H_2S environments and the increased stability of FeS films, which restrict hydrogen uptake, with increasing temperature can be a factor. The temperature dependence of HIC in the absence of a film (e.g. by cathodic charging) is not well established. It would be expected that the hydrogen concentration in the steel would increase with increasing temperature but localisation associated with a hydrostatic stress component would decrease. Hence, as with trapping effects, there are competing influences with respect to a threshold for cracking. In relation to void and crack growth the increased diffusivity would play a role.

In refinery service, the indication is that HIC can occur at temperatures above 100 °C, wherever there is a liquid phase. Hence, the possibility of cracking cannot be excluded based solely on the high temperature (private communication J. Martin, BP, 2008), though this should not be confused with the process of hydrogen attack due to methane bubble formation which is envisaged in high pressure, high temperature service (typically greater than 400 °C; Vitovec 1982).

5.2.4 Effect of steel composition on hydrogen-induced cracking

There is a wealth of information on the effect of impurities on HIC (Dewsnap et al. 1987). HIC is most often associated with MnS inclusions, generally in the form of elongated stringers (often referred to as Type 2) and control of processing to limit segregation, use of ultra-low S steels (less than 0.002 mass %), adoption of normalising heat treatment and calcium additions to provide sulphide shape control can all reduce the likelihood of failure. However, it was recognised that a decrease in oxide and oxysulphide colonies was also required and that for very severe charging conditions, interfaces in pearlite colonies could open up. With residual or applied stress, these measures to control inclusion density and shape would not be considered sufficient as SOHIC can develop from stronger interfaces in pearlite colonies at modest fugacities.

In some of the older literature there is reference to the beneficial effect of other particles in the steel (Dewsnap et al. 1987), e.g. nitrides acting as trap sites and minimising the concentration at inclusions. This is true when the amount of hydrogen is limited (as when the source is welding) or when the charging conditions are initially severe but the severity reduces quickly with time. The effect of the traps in these cases can be to soak up the limited amount of hydrogen and to slow diffusion, thus limiting void development. However, in situations where charging conditions are sustained the effect of such traps is primarily to reduce the diffusion rate and possibly the crack growth rate; they do not stop cracking.

Alloying elements that contribute to a more stable film will reduce hydrogen uptake although the studies reported by Dewsnap et al. (1987) on Cu, Cr and Ni relate to H_2S environments. The authors conclude that the evidence is strong only for copper.

There has been much research into developing HIC resistant steels (Herrmann et al. 2005) and recommended chemical compositions for steel grades up to X70 are given in ISO 3183 (2007). For X80 steel a recommended composition for mildly sour service is quoted by Herrmann et al. 2005) in mass % as: C < 0.1, Mn < 1.45, Si < 0.45, P < 0.02, S < 0.003, Nb < 0.055, Cu < 0.4, N < 0.01, Al 0.02-0.06, Ca 0.001-0.006.

5.2.5 Effect of microstructure on hydrogen-induced cracking and stress oriented hydrogen-induced cracking

Poor HIC resistance is found for banded pearlite and anomalous structure. The latter refers to low temperature transformation products, martensite or bainite, of thickness 10 μm lying parallel to the surface. The hardness would be about 450 HV and the region a site of solute segregation with Mn and P enrichment (a martensite former). When taking into account the perceived mechanism of HIC, it would seem likely that the local hardness of the steel is the key factor, the higher hardness encouraging hydrogen localisation because of the greater magnitude of the hydrostatic stresses and greater localisation of slip.

The effect of Mn and P on susceptibility to HIC is illustrated in Fig. 15.

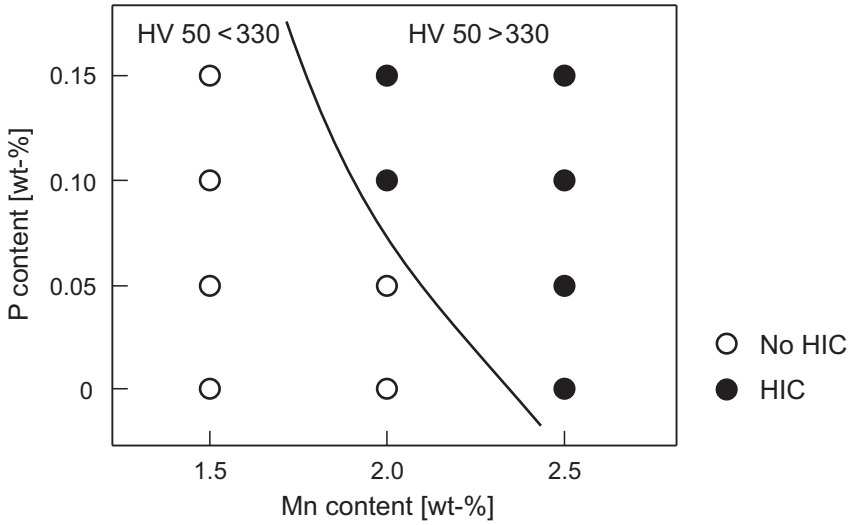

Fig. 15: HIC susceptibility defined by hardness of segregation areas in relation to relative amounts of P and Mn (Li et al. 1966 and Toyama & Konda 1989).

Acicular ferrite steels also have relatively poor resistance to HIC. It is suggested that these steels contain a mixture of structures including polygonal ferrite, upper bainite, lower bainite, auto-tempered martensite and untempered martensite with retained austenite. Tempering of these steels results in decomposition of martensite islands to cementite with some relaxation of internal stress.

Normalising and quenching and tempering offer improved resistance, with the former, in producing a fine ferrite-pearlite structure, being more effective than the tempered martensite formed by quenching and tempering. The latter has little effect on segregation because of slow diffusion and the size of the bands. For quenching and tempering to be wholly effective, it is claimed that super low sulphur steel and shape control are necessary (Li et al. 1966).

In relation to SOHIC, Pargeter (2007) notes that the susceptibility is less dominated by inclusions. Pearlite colonies and banded structures are more prone to SOHIC but there was less convincing evidence for the role of martensite islands and the role of Nb precipitates in Nb-containing steels was indicative rather than definitive.

The outer, commonly softer, regions of weld HAZs are considered to be particularly susceptible to SOHIC, though slight variations on this depending on the peak residual stress may arise. This

would seem to be rationalised from FE analysis on the basis "that through-thickness stresses peaked in the softest zone, at mid-thickness, under the influence of cross-weld applied load, due to strain concentration". As noted in Section 4.1 such concentration of strain in the soft zone would be less likely with residual stress, the relevant source of stress for the canister.

From the perspective of the canister steel where the charging conditions are mild, HIC would be considered extremely unlikely for a modern steel on the basis of Fig. 14, and, in principle, HIC resistant steels could be used so SOHIC would be the main concern. In optimising the micro-structure for resistance to HIC and SOHIC, clean steels with a homogenous microstructure are favoured; heavily banded ferrite:pearlite steels being at greatest risk. Quenched and tempered and thermo-mechanically controlled process steel are considered more resistant but with a caveat that careful welding is required to minimise softening that may render the HAZ susceptible.

The residual stresses would be assumed to be at yield, high temperature post-weld heat treatment is not an option, but some lower temperature bake out of hydrogen is feasible, so the key issue is the threshold hydrogen content/charging conditions required to induce SOHIC at these high stresses in the HAZ of welds. It is necessary to assume also that there may be a notch at the toe of the weld perhaps due to undercut that may induce some localisation of hydrogen. Localisation may also arise from triaxial stress states in the HAZ and more specifically at stress concentrators associated with particles or phase boundaries. Grinding (but minimising residual stress and unfavourable microstructure) and weld profiling would remove stress localisation due to notches at the external surface but is not feasible at the root.

5.2.6 Effect of mechanical properties on hydrogen-induced cracking

HIC is not confined just to low strength steels but has been observed over a range of yield strengths from 294 MPa – 784 MPa as noted in Section 4. Nevertheless, there did not seem to be any specific correlation of HIC resistance with strength level, other factors such as MnS inclusion density having a greater influence and perhaps masking any effect. There are conflicting effects of strength level insofar as a higher pressure of hydrogen is needed to cause local deformation in a higher strength steel but the localisation of hydrogen can become greater because of the greater hydrostatic stress.

5.2.7 Effect of weldments on hydrogen-induced cracking and stress oriented hydrogen-induced cracking

In the literature reviewed by Dewsnap et al. (1987), there was no indication of cracking in the weld metal itself in any reported service failure and also in laboratory tests, the low susceptibility being attributed to the dendritic structure and spheroidal inclusions. The weld metal could act as a crack arrester. HIC could be found in the HAZ and parent steel while as noted in Section 5.2.5, SOHIC can arise in the HAZ.

5.3 Summary of Section 5

- The threshold stress intensity factor, K_{th}, for steels in hydrogen charging environments similar to that for the waste canister will be high, at least 71 MPa $m^{1/2}$, and with control of weld hardness and accounting for the elevated exposure temperature, should exceed 100 MPa $m^{1/2}$.
- Assuming the largest weld defect that conceivably could be missed by non-destructive examination, the maximum value of K, 55 MPa $m^{1/2}$, is still significantly lower than the expected K_{th}.
- Pit depths of 1 cm in the canister wall are suggested as possible within 1'000 year exposure and with simple calculations assuming a hemi-spherical pit and high residual stress associated with high hardness, a value for K of about 81 MPa $m^{1/2}$ can be projected. However, the aspect ratio for the pit is expected to be very low and not as severe as a hemi-spherical pit but local variation in topography within the pit means that this should not be relied upon. The key is to minimise residual stress and to minimise hardness in the HAZ of the weld.
- The transition from a pit to a crack is not simply represented by a value for K as other factors such as dynamic strain (stimulated by the growing pit itself) may play a role. However, pit growth rate will be very low and any associated strain rate would correspondingly be very low and unlikely to have an influence on crack initiation.
- HIC and SOHIC are feasible failure mechanisms, in principle, for lower strength steels. A lower bound threshold level of lattice hydrogen concentration for HIC that embraces a range of steel compositions and impurity levels has not been identified though for a modern steel the threshold lattice hydrogen concentration is projected to be about 60 times the lattice hydrogen concentration estimated for these waste containment conditions. SOHIC could be initiated at lower concentrations because of the additional dependence on stress. However, laboratory testing and field exposure suggest that severe charging typical of acidic solution with H_2S is required. Nevertheless, there is good understanding of the role of microstructure on HIC and SOHIC that should allow a conservative approach to avoidance.

6 Summarised assessment of the potential for cracking

- Low strength carbon steel of the type projected for the nuclear waste canister can be envisaged to fail by a hydrogen assisted cracking mechanism only if the following conditions prevail: the hydrogen content exceeds the threshold for HIC or SOHIC; welding leads to high hardness and residual stress in combination with a large defect and dissolved hydrogen content such that K_{th} is exceeded.
- Assuming that hydrogen gas pockets with a pressure of 10 MPa exist as predicted then the lattice hydrogen solubility at 90 °C in equilibrium would be about 0.03 ppm. This is likely to be a maximum value, a progressive lowering of temperature reducing this over time to 0.01 ppm. Film formation may also reduce the concentration but cannot be assured. There are no data at this temperature that allow determination of the dissolved hydrogen generated electrochemically but there is no basis for thinking it would be larger than for the gas, even allowing for some possible effect of sulphur species.
- In relation to HIC or SOHIC, there are insufficient data to define a lower bound lattice concentration below which cracking could not develop irrespective of the steel composition and impurity level, and stress in the case of SOHIC. Thus, we cannot conclude *a priori* that these mechanisms are not feasible for the waste canister with a lattice concentration of 0.03 ppm. Nevertheless, their occurrence can be prevented by appropriate materials selection and welding practice, noting that for a modern steel the threshold lattice hydrogen concentration is projected to be about 60 times the lattice hydrogen concentration estimated for these waste containment conditions.
- The threshold stress intensity factor, K_{th}, for steels in hydrogen charging environments similar to that for the waste canister will be high, at least 71 MPa $m^{1/2}$ at ambient temperature and greater at elevated temperature.
- Assuming a maximum 2 mm crack-like defect from welding (since the internal surface of the closure weld cannot be ground) this implies that a residual stress in the HAZ of at least 896 MPa would be required for cracking to occur. Such stresses are not feasible for the carbon steels and welding practice envisaged for this application.
- Assessing the significance of deep pits in relation to cracking propensity is less straightforward. Pit depths of 1 cm in the canister wall are suggested as being possible within 1'000 years. Simple calculations for the stress intensity factor for a hemi-spherical pit would suggest that a residual stress level of 598 MPa would be required for the stress intensity factor to be 71 MPa $m^{1/2}$. The aspect ratio for the pit is expected to be smaller than a hemi-spherical pit but it could be argued that local variation in topography within the pit means that this should not be relied upon. Also, the pit-to-crack transition is not simply related to a threshold pit size but depends on other factors such as the ratio of the pit growth rate to the crack growth rate. Whilst very unlikely that pitting in combination with hydrogen uptake could lead to crack initiation in this circumstance, it is prudent to minimise the hardness of the HAZ to limit the maximum residual stress and reduce the risk.
- In terms of the period of exposure, the susceptibility will probably be greatest in the long-term where the temperature is about 50 °C, despite the projected lower concentration of dissolved hydrogen, for the following reasons: the data of Fig. 12 showing decreased K_{th} with decrease in temperature; the hydrogen profile through thickness will approach uniformity (and thus attain maximum at root weld defects); pit depths could be large and trapped hydrogen concentration tends to increase with decreasing temperature. The signifycance of the last of these statements is less certain. This uncertainty arises because the kinetics of hydrogen generation and the absorption of hydrogen will be greatest at the

elevated temperature of about 90-100 °C, where active sulphide species may participate and where uniform wetting is prevalent (limiting delocalisation). Thus the maximum in the sub-surface lattice concentration of hydrogen (C_0) is likely for this condition. In the absence of specific data for C_0 at different temperatures it is not possible to estimate the likely trapped hydrogen concentration assuming different types of traps and associated binding energies.

7 Mitigation strategies to minimise likelihood of cracking associated with hydrogen

The two primary options for further reducing the risk of hydrogen assisted cracking are control of the material and minimising the residual stress from welding.

HIC and SOHIC would not be expected for a modern steel in the relatively mild environments associated with the waste containment. The environment would be classified in the low susceptibility category in the API guideline (API 581 2000). Nevertheless, there are measures that can be taken in terms of material composition and impurity level to ensure that damage could not develop even if there were some unexpected excursion in sulphide concentration in combination with locally acidic conditions, e.g. at the extremities of a corrosion pit in the early aerobic stage. Thus, for HIC, control of processing to limit segregation, use of clean steels, adoption of normalising heat treatment and calcium additions to provide sulphide shape control can all reduce further the likelihood of crack development. Given the low severity of the environment and the relatively low hydrogen content expected the adoption of ultra-low S steel (less than 0.002 mass %), though an option, would be unnecessary.

In terms of basic composition of the steel, guidance from ISO 3183 (2007) for pipeline steels in sour environments is appropriate. The BP internal specification (BP Group 2005) for their Z-quality steel plate provides a useful reference basis for minimising risk of any sulphide induced cracking in relatively low severity conditions. In that context, the steel plate shall meet BS EN 10028-3 or equivalent steel grades. The steel making process shall require a low sulphur and low phosphorous refining process, for example in an electric furnace with double de-slagging or in the basic oxygen furnace (BOF). The steel shall be vacuum degassed whilst molten. For the chemical composition, the following supplementary requirement shall apply (mass %): C: 0.2 max, S: 0.008 max, P: 0.025 max with a maximum carbon equivalent (CE) of 0.43, based on product analysis and using the relationship:

$$CE = C + \frac{Mn}{6} + \frac{Cr + Mo + V}{5} + \frac{Ni + Cu}{15} \qquad (19)$$

The BP guidance notes that rare earth metals are not permitted.

Other factors to be considered, for SOHIC resistance, are avoidance of heavily banded ferrite:pearlite regions. Normalisation of the steel to induce homogeneity is advised.

A decision on whether to use wrought or cast steel for the waste canister is yet to be made. A cast steel is likely to have larger inclusions (these should be more broken up in processing of wrought steel), which is undesirable and interdendritic pores may be formed. However, in the main region of concern, which is the weld, the microstructure will be determined predominantly by the welding procedure and not by whether it is wrought or cast steel.

In relation to the closure weld for sealing of the cap to the cylindrical canisters, the key requirement is to minimise hardness and residual stress. Control of hardness is through materials selection as defined by the carbon equivalent and welding procedure. The BP internal specification for pipework limits hardness to 200 HBW (i.e. Brinel Hardness using WC indenter), approximately 15 Rc, and this would seem a reasonable basis for the canister. Hardness tests should be conducted to ensure adherence to specification.

This combination of refined material selection and welding is designed to a take a very low risk situation with respect to HIC and SOHIC and reduce it further.

There then remains the issue of hydrogen assisted cracking if a deep pit acts as a suitable stress concentrator. Using conversions to yield strength (www.woodcousa.com/conv_chart.htm) the maximum values set for the hardness, 200 HBW, would suggest a maximum tensile strength of about 660 MPa. The yield strength relative to tensile strength will depend on the particular steel composition but for mild steel it is unlikely to exceed 75 % of the tensile strength (www.tppinfo.com/defect_analysis/yiled_strength.html). This suggests a maximum yield strength of hardened steel in the HAZ of 495 MPa and by inference the maximum residual stress. On this basis, the stress intensity factor for the 1 cm deep pit described in Section 5.1 would be limited to 59 MPa $m^{1/2}$, now significantly below the threshold for hydrogen assisted cracking.

It will be assumed that appropriate inspection using ultrasonic methods and radiography is employed following welding to identify any significant defects (within the constraints of managing "hot" waste). The same should be applied to the cast parent steel to characterise porosity. Tensile test data for the material should be obtained at different depths to ensure conformation with specification.

Although treatment of the weld root is not feasible, grinding of the weld cap should be undertaken to ensure a smooth profile and minimise stress concentration at the weld toe. The grinding should be done carefully to minimise grinding-induced residual stress.

Modern welding practice should eliminate the possibility of hydrogen cracking from the welding process itself. Hydrogen can be introduced from moisture in the electrodes, from flux, and from contaminants and rust on the canister surface or on welding wires. Cleanliness, use of gas-shielded metal-arc welding and careful choice of coatings or fluxes should minimise the possibility.

8 Concluding remarks

The analysis in this report is quite conclusive and the strategy evoked will confidently eliminate the risk of a cracking of the waste canisters due to absorbed hydrogen. Nevertheless, there would be added value in selective measurements that further bolster the conclusions.

- Evaluate the impact of welding procedure specification for the closure weld (including surface grinding) by sectioning and characterising the microstructure and measuring hardness distribution and residual stress in a reference canister. Perform a similar evaluation but near-surface on a ground weld. These measurements should be considered a requirement and not optional.
- Determine lattice hydrogen uptake and the hydrogen diffusion coefficient for the class of steel under simulated exposure environments at 90 °C and at 50 °C and check against the assumed values for this analysis.
- In that context, the tests should be done with and without sulphur species with the latter based on separate calculation and/or measurement of likely concentration and form of the sulphur species at the reacting surface (taking account of transport) for different exposure times.
- Evaluate the kinetics for reduction of sulphate at 90 °C.
- More information on the time-evolution of the local concentrations of various species at the waste containment steel surface and the reactant supply kinetics and the impact on surface films would be enlightening.

9 References

API 581 (2000): Risk-based inspection resource document. 1st edition, American Petroleum Institute.

Asher, S. & Singh, P.M. (2008): Hydrogen production and permeation in near-neutral pH environments. Corrosion 2008, Paper no. 08411. NACE Int., Houston.

Beachem, C.D. (1972): A new model for hydrogen assisted cracking (hydrogen embrittlement). Metall. Trans. 3, 437-451.

Birnbaum, H.K. (1990): Mechanisms of hydrogen-related fracture of metals. *In*: Gangloff, R.P & Ives, M.B. (eds.): Environment Induced Cracking of Metals. NACE-10. NACE Int. Houston.

Bockris, J.O'M. & Subramanyan, P.K. (1971): Thermodynamic analysis of H in metals in the presence of an applied stress field. Acta Metall. 19, 1205-1218.

Boellinghaus, T., Hoffmeister, H. & Dangeleit, A. (1995): A scatterband for hydrogen diffusion coefficients in micro-alloyed and low carbon structural steels. Welding in the World 35, 83-96.

BP Group (2005): Guidance on practice for materials for sour service. BP Group Document No. GP 06-20.

Castenada, H. & Leis, B.N. (2007): Hydrogen entry mechanism for API X-65 steel exposed in near neutral solutions under adsorption-activation conditions. Corrosion 2007. NACE Int., Houston.

Cheng, Y., Yang, L. & King, F. (2000): Analysis of hydrogen permeation through pipeline steel in near-neutral pH SCC environments. Proc of IPC 2000, Calgary, Canada.

Coe, F.R. (1973): Welding steels without hydrogen cracking. The Welding Institute.

Crank, J. (1975): The mathematics of diffusion. Oxford Science Publications, 2nd Edition. Oxford University Press.

Cristensen, C. (1999): SOHIC – So what. Corrosion 1999, Paper No. 434. NACE Int., Houston.

Curti, E. & Wersin, P. (2002): Assessment of porewater chemistry in the bentonite backfill for the Swiss SF / HLW Repository. Nagra Technical Report NTB 02-09. Nagra, Wettingen, Switzerland.

Dewsnap, R.S., Jones, C.L., Lessells, J., Morrison, W.B., Rudd, W.J., Walker, E.F. & Wilkins, R. (1987): A review of information on hydrogen induced cracking and sulphide stress corrosion cracking in linepipe steels. Offshore Technology Report OTH 86 256. HMSO.

Elboujdaini, M., Revie, R.W. & DeRushi, C. (2003): Effects of metallurgical parameters and non-metallic inclusions on behaviour for oil and gas industry steels on hydrogen induced cracking. Corrosion 2003, Paper no 03528, NACE Int., Houston.

Féron, D. & Macdonald, D.D. (eds.) (2003): Prediction of long term corrosion behaviour in nuclear waste systems. EFC No 36, IOM^3.

Ferreira, P.J., Robertson, I.M. & Birnbaum, H.K. (1998): Hydrogen effects on the interaction between dislocations. Acta Mater. 46, 1749-1757.

Gangloff, R.P. (1986): A Review and analysis of the threshold for hydrogen environment embrittlement of steel. *In*: Levy, M. & Isserow, S. (eds.): Corrosion Prevention and Control. 33rd Sagamore Army Materials Research Conference. US Army Laboratory Command, Watertown, MA, 61-111.

Gangloff, R.P. (2003): Hydrogen assisted cracking. *In*: Milne, I., Ritchie, R.O., Karihaloo, B. (eds): Comprehensive Structural Integrity 6, 31-102. Elsevier.

Gangloff, R.P. (2008a): Science-based prognosis to manage structural alloy performance in hydrogen. Presented at Effects of Hydrogen on Materials, Jackson Lake Lodge, Wyoming, September 2008.

Gangloff, R.P. (2008b): Critical issues in hydrogen assisted cracking of structural alloys. *In*: Shiplov, S.A., Jones, R.H., Olive, J.-M. & Rebak, R.B. (eds.): Environment-Induced Cracking of Materials. Banff, Canada, September 2004. Elsevier, pp. 141-165.

Gerberich, W.W., Livne, T., Chen, X.-F. & Kaczorowski, M. (1988): Crack growth from internal hydrogen - Temperature and microstructural effects on 4340 steel. Metall. Trans. 19A, 1319-1344.

Grabke, H.J. & Riecke, E. (2000): Absorption and diffusion of hydrogen in steels. Mater. Technol. 34, 331-342.

Gradstein, I.S. & Ryzhik, I.M. (1994): Table of integrals, series and products. 5th Edition. Academic Press, San Diego – New York – London.

Griffiths, A.J., Hutchings, R.B. & Turnbull, A. (1994): Hydrogen uptake and transport in low alloy steels. Proc. of Second International Conference on Interaction of Pipeline Steels with Hydrogen in Petroleum Industry Pressure Vessel and Pipeline Service. Vienna, October 1994.

Han, J., Yang, Y., Nesic, S. & Brown, B.N. (2008): Roles of passivation and galvanic effects on localized CO_2 corrosion of mild steel. TITLE. Corrosion 08, Paper no. 08332. NACE. Int. Houston.

Hasegawa, M. & Osawa, M. (1980): Anomalous corrosion of austenitic stainless steel exposed to high temperature and pressure. Corrosion 36, 67-73.

Herrmann, T., Bosch, C. & Martin, J.W. (2005): HIC assessment of low alloy steel line pipe for sour service application – literature survey. 3R International 44/7, 409-417.

Hinton, B.R.W. & Proctor, R.P.M. (1983): The effect of strain rate and cathodic protection on the tensile ductility of X-65 pipeline steel. Corrosion Science 23, 101-123.

Iino, M. (1978): The extension of hydrogen blister-crack array in linepipe steels. Metall. Trans. 9, 1581-1590.

ISO 15156-2 (2003): Petroleum and natural gas industries – Materials for use in H_2S-containing environments in oil and gas production. Part 2.

ISO 3183 (2007): Petroleum and natural gas industries – steel pipe for pipeline transportation systems. ISO, Geneva.

ISO 17081 (2007): Method of measurement of hydrogen permeation and the determination of hydrogen uptake and transport in metals by an electrochemical technique.

Jeffrey, A. (1995): Handbook of mathematical formulas and integrals. Academic Press, San Diego – New York – London.

Johnson, H.H. (1988): Hydrogen in iron. Metal. Trans. 19A, 2371-2387.

Johnson, L. & King, F. (2003): Canister Options for the Disposal of Spent Fuel. Nagra Technical Report NTB 02-11. Nagra, Wettingen, Switzerland.

Johnson, L. & King, F. (2008): The effect of the evolution of environmental conditions on the corrosion evolutionary path in a repository for spent fuel and high-level waste in Opalinus Clay. J. Nucl. Mater. 379, 9-15.

JNC (2000): H12: Project to establish the scientific and technical basis for HLW disposal in Japan. Japan Nuclear Development Institute JNC/TN 1410.

Kawai, S. & Kasai, K. (1995): Fatigue Fracture Engineering. Mater. Struct. 8, 115-127.

King, F. & Stroes-Gascoyne, S. (2000): An assessment of the long-term corrosion behaviour of C-steel and the impact of the redox conditions inside nuclear fuel waste disposal container. Report No. 06819-REP-01200-10028-R00. Ontario Power Generation Nuclear Waste Management Division.

Kiuchi, K. & McLellan, R.B. (1983): The solubility and diffusivity of hydrogen in well-annealed and deformed iron. Acta Metall. 31, 961-984.

Kocak, M., Hadley, I., Szavai, S., Tkach, Y. & Taylor, N. (eds.) (2008): FITNET, Section 9: Corrosion Damage Module. GKSS, Germany.

Kondo, Y. (1989): Prediction of fatigue crack initiation life on pit growth. Corrosion 45, 7-11.

Landolt, D., Davenport, A., Payer, J. & Shoesmith, D. (2009): A review of materials and corrosion issues regarding canisters for disposal of spent fuel and high-level waste in Opalinus Clay. Nagra Technical Report NTB 09-02. Nagra, Wettingen, Switzerland.

Li, J.C.M., Oriani, R.A. & Darken, L.S. (1966): The thermodynamics of stressed solids. Z. Physik. Chem. 49, 271-290.

Liang, Y., Sofronis, P. & Dodds, R. (2004): Interaction of hydrigen with crack-tip plasticity: effects of constraint on void growth. Materials Science and Engineering A/366, 397-411.

Lynch, S.P. (2007): Progress towards understanding mechanisms of hydrogen embrittlement and stress corrosion cracking, Corrosion 2007, Paper no. 07493. NACE Int., Houston.

Magnin, T. & Najjar, D. (1995): Influence of surface defects on hydrogen effects during stress corrosion and corrosion fatigue. *In*: Turnbull, A. (ed.): Hydrogen Transport and Cracking in Metals. Institute of Materials, 38-49.

Murakami, Y. (2008): Structural issues in development of hydrogen energy infrastructure in Japan. Presented at Effects of Hydrogen on Materials, Jackson Lake Lodge, Wyoming, September 2008.

Murray, G.T. (1988): Prevention of hydrogen embrittlement by surface films. *In*: Raymond, L. (ed.): Hydrogen Embrittlement – Prevention and Control. ASTM STP 262, 304-317.

Newman, J.F. & Shreir, L.L. (1969): Effect of cabon content and structure of steels on solubility and diffusion coeffcient of hydrogen. JISI 207, 1369-1372.

Oriani, R.A. (1990): Hydrogen effects in high strength steels. *In*: Gangloff, R.P & Ives, M.B. (eds.): Environment Induced Cracking of Metals. NACE-10. NACE Int., Houston.

Pargeter, R.J. (2007): Susceptibility to SOHIC for linepipe and pressure vessel steels – Review of current knowledge. Corrosion 2007. NACE Int., Houston.

Pourbaix, M. (1996): Atlas of electrochemical equilibria in aqueous solutions. Pergamon Press.

Robertson, I. (2008): Revealing the fundamental processes controlling hydrogen embrittlement. Presented at Effects of Hydrogen on Materials, Jackson Lake Lodge, Wyoming, September 2008.

San Marchi, C. & Somerday, B.P. (2008): Technical reference on hydrogen compatibility of materials. Sandia Report SAND2008-1163. Sandia National Laboratoires, Albuquerque, New Mexico and Livermore, California. www.ca.sandia.gov./matlsTechRef/.

San Marchi, C., Nibur, K., Balch, D., Somerday, B., Tang, X., Schiroky, G. & Michler, T. (2008): Hydrogen-assisted fracture in austenitic stainless steels. Presented at Effects of Hydrogen on Materials, Jackson Lake Lodge, Wyoming, September 2008.

Senger, R. & Ewing, J. (2008): Evolution of temperature and water content in the bentonite buffer: Detailed modelling of two-phase flow processes associated with the early closure period. Nagra Arbeitsbericht. Nagra, Wettingen, Switzerland.

Smart, N.R., Blackwood, D.J. & Werme, L. (2002a): Anaerobic corrosion of carbon steel and cast iron in artificial groundwater. Part 1. Electrochemical aspects. Corrosion 58, 547-557.

Smart, N.R., Blackwood, D.J. & Werme, L. (2002b): Anaerobic corrosion of carbon steel and cast iron in artificial groundwater. Part 2. Gas generation. Corrosion 58, 627-637.

Takeuchi, I., Kushida, T., Okaguchi, S., Yamamoto, A. & Miura, M. (2004): Development of high strength line pipe steel for sour service and full ring evaluation in sour environment. Proc. of OMEA 2004 (*cited in Herrmann et al. 2005*).

Taniguchi, N., Honda, A. & Ishikawa, H. (1998): Experimental investigation of passivation behaviour and corrosion rate of carbon steel in compacted bentonite. Mat. Res. Soc. Symp. 506. Materials Research Society.

Toyama, K. & Konda, N. (1989): Environmental effects on fatigue crack initiation. *In*: Evaluation of Materials Performance in Severe Environments. ISIJ 1, 105-112. Kobe, Japan, November 1989.

Turnbull, A. (1983): The solution composition and electrode potential in pits, crevices and cracks. Corros. Sci. 23, 833-870.

Turnbull, A. (1993): Modelling of environment-assisted cracking. Corros. Sci. 34, 921-960.

Turnbull, A. & Zhou, S. (2001): Environment assisted cracking of steam turbine steels – Modelling of crack electrochemistry. Corrosion 2001, Paper No. 01237. NACE, March 2001.

Turnbull, A. & Zhou, S. (2004): Pit to crack transition in stress corrosion cracking of a steam turbine disc steel, Corrosion Science. Corros. Sci. 46, 1239-1264.

Turnbull, A., Hutchings, R.B. & May, A.T. (1989): The effect of temperature and H_2S concentration on hydrogen transport and cracking in a 13 % chromium martensitic stainless steel. Proc. of Conf. on Hydrogen Effects on Materials Behaviour, Wyoming, September 1989.

Turnbull, A., Zhou, S., Nicholson, P. & Hinds, G. (2008): Chemistry of concentrated salts formed by evaporation of seawater on duplex stainless steel. Corrosion 64, 325-333.

Vitovec, F.H. (1982): Modeling of hydrogen attack of steel in relation to material and environmental variables. *In*: Interrannte, C.G. & Pressouyre, G.M. (eds.): Current Solutions to Hydrogen Problems in Steels. ASM, Metals Park, Ohio, pp 236-248.

Yu, J.G., Luo, J.L. & Norton, P.R. (2001): Effects of hydrogen on the electronic properties and stability of the passive films on iron. Applied Surface Sci. 177, 129-138.

Zakroczymski, T. (1985): Entry of hydrogen into iron alloys from the liquid phase. *In*: Oriani, R.A., Hirth, J.P. & Smialowski, M. (eds.): Hydrogen Degradation of Ferrous Alloys. Noyes Publications 1985, 215-288.

APPENDIX

Approximate calculation of hydrogen pressure build up inside canister

1 Diffusion through a flat plate

Consider the diffusion of hydrogen atoms from the exterior surface of a hollow cylindrical canister through the walls, having thickness h, into the sealed interior. The inner radius of the cylindrical wall is denoted by R and the internal canister length by L. The end plates are assumed to be flat and they are clearly circular. Initially, the concentration of hydrogen atoms in the containing walls is assumed to have the same value C_2. The concentration of hydrogen atoms at the external surface is assumed to be held at a fixed value denoted by $C_1 > C_2$. It is first required to estimate the concentration distribution for hydrogen atoms in the interior of the canister as a function of time. The time dependent concentration of hydrogen atoms on the interior surface is denoted by C(t) where t is the elapsed time. The first approximation to be made is that $C(t) = C_2$ for all times. By taking $C_2 = 0$ an over-estimate of the flux of hydrogen atoms at the inner wall of the container into the gas will be obtained. The second approximation that is made is to assume that the cylinder radius R is much larger than the wall thickness h so that the curved walls of the cylinder can be approximated by a flat plate having thickness h. This avoids having to numerically estimate zeroes of a transcendental equation involving Bessel functions that arise when solving the equivalent axi-symmetric problem (see Crank 1975, Section 5.4). The first five of the required zeroes are given in Crank (1975, Tab. 5.3) but these may not be sufficient for the adequate convergence at short times of the associated infinite series that generates the required solution.

The concentration distribution of hydrogen atoms within the canister walls is denoted by c(x,t) and is assumed to satisfy the one-dimensional form of the standard diffusion equation

$$\frac{\partial c}{\partial t} = D\frac{\partial^2 c}{\partial x^2}, \qquad \text{(A1)}$$

where D is the diffusion coefficient for transport of hydrogen atoms in the wall. The external and internal surfaces are located at x = 0 and x = h respectively and the initial and boundary conditions are written

$$\begin{aligned} &c(x,0) = C_2\ , \quad 0 < x < h\ , \\ &c(0,t) = C_1\ , \qquad t > 0\ , \\ &c(h,t) = C_2\ , \qquad t > 0\ . \end{aligned} \qquad \text{(A2)}$$

The problem posed has been solved (Crank 1975, Section 4.3.1) and the solution, using the above conditions and notation, is given by

$$c(x,t) = C_1 - (C_1 - C_2)\left[\frac{x}{h} + \frac{2}{\pi}\sum_{n=1}^{\infty}\frac{1}{n}\sin\left(\frac{\pi n x}{h}\right)\exp\left(-\frac{D\pi^2 n^2 t}{h^2}\right)\right]. \qquad \text{(A3)}$$

The initial condition in (A2) is satisfied because (Gradstein & Ryzhik 1994, Section 1.441)

$$\sum_{n=1}^{\infty} \frac{\sin(ny)}{n} = \frac{\pi - y}{2}, \quad 0 < y < 2\pi, \tag{A4}$$

so that

$$\frac{2}{\pi}\sum_{n=1}^{\infty} \frac{1}{n}\sin\left(\frac{\pi n x}{h}\right) = 1 - \frac{x}{h}. \tag{A5}$$

The remaining boundary conditions in (A2) are clearly satisfied by the solution (A3). To check that (A3) is a solution of (A1) it is sufficient to note that

$$\frac{\partial c(x,t)}{\partial t} = D\left(C_1 - C_2\right)\frac{2\pi}{h^2}\sum_{n=1}^{\infty} n\sin\left(\frac{\pi n x}{h}\right)\exp\left(-\frac{D\pi^2 n^2 t}{h^2}\right), \tag{A6}$$

$$\frac{\partial^2 c(x,t)}{\partial x^2} = \left(C_1 - C_2\right)\frac{2\pi}{h^2}\sum_{n=1}^{\infty} n\sin\left(\frac{\pi n x}{h}\right)\exp\left(-\frac{D\pi^2 n^2 t}{h^2}\right). \tag{A7}$$

It is clear that the first two terms on the R.H.S. of (A3) represent the steady state solution, which is linear in the through-thickness variable x.

At time t, the flux of hydrogen atoms J(t) across the internal surface of the canister into the contained gas is given by

$$J(t) = -D\frac{\partial c(x,t)}{\partial x}\bigg|_{x=h} = \frac{D\left(C_1 - C_2\right)}{h}\left[1 + 2\sum_{n=1}^{\infty}(-1)^n \exp\left(-\frac{D\pi^2 n^2 t}{h^2}\right)\right]. \tag{A8}$$

2 Application to the practical problem

Consider a cylindrical canister of internal length L where the internal radius is R, which is assumed to be much larger than the wall thickness h. The end-plates of the cylinder are of radius R and thickness h. The canister is exposed externally to hydrogen gas molecules that are adsorbed as individual hydrogen atoms (i.e. positively charged protons and associated electrons that preserve electro-neutrality) that diffuse through the wall into the interior of the canister. The outer surface concentration of hydrogen atoms is fixed having a value C_1 and the inner concentration is $C_2 < C_1$ for all times so that there is an inward flux of hydrogen atoms. The initial concentration of hydrogen atoms in the wall is C_2. The total surface area S of the interior of the canister is given by

$$S = 2\pi R^2 + 2\pi R L = 2\pi R\left(R + L\right). \tag{A9}$$

The volume V of the internal space when the canister is empty is given by

$$V = \pi R^2 L. \tag{A10}$$

The volume of the contents V_c is given so that the volume of gas contained is $V - V_c$.

All the hydrogen atoms that have diffused through the wall recombine at the inner surface into hydrogen molecules that are released as hydrogen molecules into the contained gas that is assumed to be well mixed for all times t. It is assumed also that no hydrogen molecules are contained in the enclosed gas at time t = 0. Let M(t) denote the number of moles of hydrogen molecules that have entered the gas in the canister through unit surface area during a time interval t, and let $c_{H2}(t)$ denote the concentration (moles/unit volume) of the hydrogen molecules contained in the enclosed gas at time t. It then follows that

$$SM(t) = \left(V - V_c\right) c_{H2}(t). \tag{A11}$$

On using (A9) and (A10) it follows that the concentration of hydrogen molecules at time t is

$$c_{H2}(t) = \frac{2\left(1 + \dfrac{L}{R}\right)}{L - \dfrac{V_c}{\pi R^2}} M(t). \tag{A12}$$

The function M(t) relating to hydrogen molecules is obtained from the flux J(t) of hydrogen atoms on integration, as follows

$$M(t) = \frac{1}{2}\int_0^t J(\tau)\, d\tau, \tag{A13}$$

where the factor $\frac{1}{2}$ appears because two atoms of hydrogen from the cylinder wall combine at the inner surface to form one molecule of hydrogen in the contained gas. On using (A8)

$$\begin{aligned} M(t) &= \int_0^t \frac{D\left(C_1 - C_2\right)}{2h}\left[1 + 2\sum_{n=1}^{\infty} (-1)^n \exp\left(-\frac{D\pi^2 n^2 \tau}{h^2}\right)\right] d\tau \\ &= \left(C_1 - C_2\right) h\left[\frac{Dt}{2h^2} + \frac{1}{\pi^2}\sum_{n=1}^{\infty} \frac{(-1)^n}{n^2}\left\{1 - \exp\left(-\frac{D\pi^2 n^2 t}{h^2}\right)\right\}\right]. \end{aligned} \tag{A14}$$

Since (Jeffrey 1995, Section 1.8.3.4)

$$\sum_{n=1}^{\infty} \frac{(-1)^n}{n^2} = -\frac{\pi^2}{12}, \tag{A15}$$

the result (A14) may be expressed in the form

$$M(t) = \left(C_1 - C_2\right) h\left[\frac{Dt}{2h^2} - \frac{1}{12} - \frac{1}{\pi^2}\sum_{n=1}^{\infty} \frac{(-1)^n}{n^2} \exp\left(-\frac{D\pi^2 n^2 t}{h^2}\right)\right]. \tag{A16}$$

Substitution in (A12) then leads to the result

$$c_{H2}(t) = \frac{(C_1 - C_2)\left(1 + \frac{L}{R}\right)\frac{h}{L}}{1 - \frac{V_c}{\pi R^2 L}} \left[\frac{Dt}{h^2} - \frac{1}{6} - \frac{2}{\pi^2} \sum_{n=1}^{\infty} \frac{(-1)^n}{n^2} \exp\left(-\frac{D\pi^2 n^2 t}{h^2} \right) \right] . \quad \text{(A17)}$$

It should be noted that $c_{H2}(t) \to 0$ as $t \to 0$, as required, because of the relation (A15).